Science of the Total Environment 735 (2020) 139303

Contents lists available at ScienceDirect

Science of the Total Environment

journal homepage: www.elsevier.com/locate/scitotenv

# Urban climate assessment in the ABC Paulista Region of São Paulo, Brazil

María Cleofé Valverde [a,*], Lúcia Helena Coelho [a], Andréa de Oliveira Cardoso [a], Humberto Paiva Junior [a], Ricardo Brambila [b,1], Cláudia Boian [a], Paula Cristina Martinelli [c,2], Natasha Murgu Valdambrini [d]

[a] Centre of Engineering, Modelling and Applied Social Sciences, Federal University of ABC, Avenida dos Estados, 5001, Santo André, SP 09210-580, Brazil
[b] Environmental and Urban Systems Integration Laboratory, Federal University of ABC, Brazil
[c] Municipal Secretary of Environment for Lorena, São Paulo, Brazil
[d] Federal University of ABC, Avenida dos Estados, 5001, Santo André, SP, 09210-580, Brazil

## HIGHLIGHTS

- The Heat island and greenhouse gas emissions in an industrial region
- The Urban Climate System in the ABC Paulista region of São Paulo, Brazil
- Vehicular emissions and levels air quality in the ABC Paulista region of São Paulo
- The sea and land breezes and relationship with the heat island

## GRAPHICAL ABSTRACT

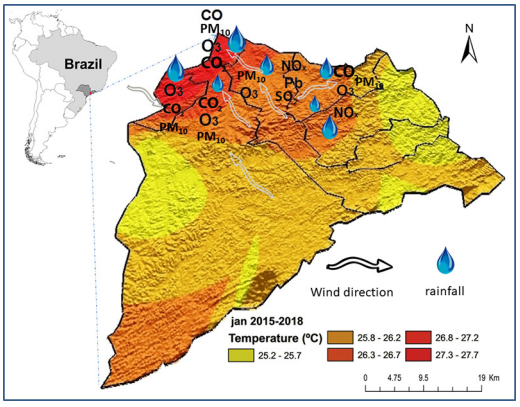


## ARTICLE INFO

*Article history:*
Received 29 December 2019
Received in revised form 6 May 2020
Accepted 7 May 2020
Available online 19 May 2020

Editor: Jianmin Chen

*Keywords:*
Heat Islands
Tropospheric ozone
Particulate matter
Thermal comfort
Mixed deposition
Precipitation

## ABSTRACT

This article aims to map the urban climate in the ABC Paulista (ABCP) region, which is located in the southeast area of the Metropolitan Region of São Paulo (MRSP), Brazil. More than 80% of the ABCP urban area comprises the municipalities of Santo André (SA), São Bernardo do Campo (SBC), São Caetano do Sul (SCS), Mauá (MA), Diadema (DIA), and Ribeirão Pires. Considering a four-year dataset (2015–2018), higher urban heat island (HI) intensities were found in the spring (3.7 °C) and summer (3.2 °C), in DIA and SCS, and these HI intensities were associated with extreme thermal discomfort in the afternoon. More intense and concentrated rainfall patterns over a shorter period were identified in ABCP, especially in DIA and SCS. An analysis of $O_3$ and $PM_{10}$ at fixed pollutant monitoring stations identified SBC as having the largest number of days with $O_3$ concentrations beyond the standards; meanwhile, SCS significantly exceeded the $PM_{10}$ standards. The traffic and transportation simulation tool, Equilibre Multimodal/Multimodal Equilibrium which was used to estimate emissions from mobile sources, identified SCS as having the highest emissions rates for $CO_2$, CO, HC and $PM_{10}$. Analysis of the rainwater composition in Capuava (located along boundary of SA and MA) and Paranapiacaba (an environmental preservation area of SA) identified that a major contribution of strong acids and heavy metals in Capuava possibly originated from the Capuava Petrochemical Complex. Meanwhile, the main source of pollutants in Paranapiacaba was from the industrial city of Cubatão. Principal component analysis identified the first three components, which

* Corresponding author.
*E-mail address:* maria.brambila@ufabc.edu.br (M.C. Valverde).
[1] Address: Avenida dos Estados, 5001, Santo André, SP 09210-580, Brazil.
[2] Address: R. Comendador Custódio Vieira, 333 - Centro, Lorena - SP, 12600-030.

https://doi.org/10.1016/j.scitotenv.2020.139303

explained 80.7% of the total variance of the data and the main urban climate processes. The HI intensity was associated with thermal discomfort; moreover, the PCA showed the inverse correlation between the number of days that $O_3$ and $PM_{10}$ exceeded the limits with low relative humidity and no precipitation.



## 1. Introduction

The study of climatic phenomena at cities' surfaces which works to establish an association between urban characteristics and the local climate, is urban climatology. The urban climate develops from changes in both the surface cover and activities that may cause corresponding changes in balances of energy, water, mass and momentum (Oke, 1987; Monteiro and Mendonça, 2003; Arnfield, 2003).

Since the 1960s, several research studies have aimed to quantify and analyze urban infrastructure and the contributions of anthropogenic activities to urban and local-scale atmospheric changes (Auer, 1978; Oke et al., 1999; Grimmond, 2007). In Brazil, during the 1970 Monteiro and Mendonça (2003) created a conceptual model called the Urban Climate System (UCS) to explain the interrelationship between the use of urban space and the local climate. The UCS is defined as an open and dynamic arrangement composed of three subsystems: thermodynamic, physicochemical, and hydrometric (Monteiro and Mendonça, 2003). The thermodynamic subsystem considers heat island, cold Island, environmental thermal comfort, and thermal inversion phenomena; the physicochemical subsystem highlights air pollution, acid rain, and the relationship between urban structures and winds; and the hydrometric subsystem considers rainfall in urban areas, as well as the associated changes and impacts linked to flooding and landslides (Monteiro and Mendonça, 2003). The three subsystems aim to include the main effects observed in the climate of urban spaces; however, due to the complexity of the UCS, only a few studies have been able to assess the three subsystems in an integrated manner. Although separating the subsystems didactically simplifies the analysis, the main changes, such as the heat island and its effects, can be explained by considering the interactions among the three components.

Heat island (HI) events in urban areas are considered an immediate response to relatively high concentrations of anthropogenic heat sources in cities. Urbanization leads to the construction of buildings and residences, a reduction in green areas with the implementation of larger industrial complexes, and an increase in the vehicle transportation fleet, which results in higher pollutant emissions, increased in the absorption of solar radiation reaching the land surface, and local wind circulation changes. These factors explain the higher temperatures in urban areas in comparison to their surroundings, which establish HIs (Oke, 1987; Barros and Lombardo, 2016).

In urban centers, HI intensities can be differentiated depending on the quantification method, type and use of land occupation. When HI is quantified through the observed air temperatures, the intensity can reach up to 5 °C in dense urban areas, as found in the city of Presidente Prudente, São Paulo, Brazil (Cardoso and Amorim, 2018); however, the HI intensity also varies according to the geographical location. Santamouris et al. (2017) analyzed data from six weather stations in Sydney, Australia and found that the HI intensity can range from 0 to 11 °C due to the prevailing weather.

When considering temperatures from radiation emissions from urban surfaces using remote sensing techniques, the intensity may be much higher as found in São Paulo, Brazil (Barros and Lombardo, 2016), Beijing, China (Tran et al., 2006) and Medellin, Colombia (Peng et al., 2012), which have reached values of 8 °C, 10 °C and 7 °C, respectively. Since thermal band satellite images were used in the associated studies, many of these measurements are related to specific day and time data.

The physicochemical UCS subsystem addresses wind circulation and pollution. According to Atkinson (1981), the sea breeze is characterized by a wind intensity increase, direction change, temperature decrease and humidity increase.

Several studies in the MRSP showed that different types of circulations characterized the arrival of a breeze (Oliveira et al., 2003), with the sea breeze being the most frequent behavior recorded. The sea breeze is identified through wind direction pattern changes from NE -NW to SE, which enters São Paulo between 1:00 PM and 2:00 PM, with a simultaneous air temperature decrease, and a specific humidity and wind speed increase.

The wind in particular upholds the HI intensity: high wind velocity supports ventilation and fading of the HI phenomenon. Conversely, wind direction, is an important piece of information, as it can bring humid or dry (warm) air and cloudiness, which characterizes breeze types, influencing HI intensification or reduction.

The local circulation, breezes, HI, and synoptic flow determine pollutants concentrations and air quality. In some areas, two or more of these events may arise simultaneously and force an undesirable decrease in air quality conditions, causing polluted air entrapment near cities. Instead, sea and land breeze circulations may favor pollutant dispersion in urban areas (Freitas et al., 2007).

In metropolitan areas, vehicular emissions play a prominent role in air pollution levels, while industrial emissions significantly affect air quality in more specific regions (CETESB, 2016; Andrade et al., 2017). In the MRSP, 87% of the air pollutants' annual emissions come from mobile sources (ANTP, 2014). In 2015, mobile and stationary sources were responsible for the emission of about 167 thousand tons $year^{-1}$ of carbon monoxide (CO), 44 thousand tons $year^{-1}$ of hydrocarbons (HC), 80 thousand tons $year^{-1}$ of nitrogen oxides ($NO_x$), 5 thousand tons $year^{-1}$ of particulate matter (PM), and 7 thousand tons $year^{-1}$ of sulfur oxides ($SO_x$) (CETESB, 2016).

Gaseous pollutants and aerosols affect the irradiation balance once they are able to absorb and emit more infrared radiation. This is reflected in the temperature increase, which is especially remarkable with respect to tropospheric ozone ($O_3$) and carbon dioxide ($CO_2$) emissions (Martins and Andrade, 2008; Andrade et al., 2017).

Acid rain events are more likely related to regional specificities. Acid deposition, conventionally, has pH values below 5.6 and is associated with specific pollutants (typically $SO_2$, $H_2SO_4$, $HNO_3$, and low molecular weight carboxylic acids) produced by foundries, thermoelectric plants, petroleum refineries, vehicle engines, and industrial combustion processes. These pollutants do not remain in the air indefinitely, however; they return to the land surface as wet deposition. Thus, the concentrations of dissolved chemical species in rainwater are directly related to the prevailing weather (Brena, 2002; Dayan and Lamb, 2003). In Brazil, most acidic rainfall events were identified both in industrialized regions (Santos et al., 2007) and in rural areas (Coelho et al., 2011), through rainwater samples during different periods of the year.

Santos et al. (2007) collected rainwater samples over a period of 720 days (July 2002 to June 2004) in the city center of São Paulo, Brazil and determined that ammonium ($NH_4^+$) was the most present ion, followed by nitrate, acetate, sodium, and sulfate. These five ions represented nearly 70% of the ionic content of rainwater samples. The researchers concluded that rainwater in the central area of São Paulo is strongly influenced by local sources of air pollutants, particularly by large vehicle fleets and civil construction activities.

With respect to the rainfall pattern corresponding to the hydrometric subsystem, researchers focused not only on assessing changes in rainfall intensity and frequency but also on their impacts on urban areas. In the MRSP, several studies have shown that daily precipitation

has increased considerably in recent decades, intensifying extreme events. The effects of HIs, air pollution, and sea breeze circulations are considered possible causes of daily summer rainfall enhancement over urban areas (Xavier et al., 1994; Silva Dias et al., 2012; Marengo et al., 2013). Flooding and mass movement events are the main impacts of daily rainfall extremes, in addition to the social and environmental vulnerabilities of urban areas that increase the amount of damage caused (Nobre et al., 2011; Kermanshah et al., 2017).

Studies about urban climate in the ABC Paulista (ABCP) region are scarce and mainly related to rainfall and its extremes (Valverde et al., 2018) as well as to its impacts related to the higher occurrence of floods and landslides (Molina et al., 2015; Fernandes and Valverde, 2017). Recent studies in the urban area of ABCP showed a decrease in the total annual rainfall over the last 15 years, but with more intense and concentrated daily rainfall in the summer for short periods, especially in the municipalities of SCS, DIA, and SBC (Valverde et al., 2018).

Thermal features and the intensity of urban and intra-urban HIs were studied in two municipalities of ABCP: SBC and SA (Simeão et al., 2019; Valverde and Paiva Junior, 2018, respectively). The authors identified an urban HI with an intensity of 3 °C in the summer, while an intra-urban HI presented a lower intensity (1.5 °C). Valverde and Paiva Junior, 2018 simulated $CO_2$ emissions using a transportation model and identified SCS and SBC as the municipalities with the highest $CO_2$ emission levels from vehicles (tons $km^{-1}$ driven) due to their extensive and heavy traffic routes, which coincides with the warmest areas of these municipalities.

Volatile organic compounds (VOCs), ozone precursors in the atmosphere, were studied and analyzed near Capuava Petrochemical Complex in Mauá (MA) and Santo André (SA), indicating that the emissions sources were predominantly vehicular. Measurements of wind direction and velocity showed that the circulation breeze plays a key role in pollutants transportation in the region (Boian et al., 2015; Coelho et al., 2017).

From this scenario, this article aims to study the urban climate in the ABCP region focusing on the three subsystems of the UCS model that describe the main effects of changes in the local atmosphere and their interactions. These are the HIs, thermal comfort, sea-to-land breezes, daily rainfall intensity, air pollution, and rainwater composition.

This is the first time that the characteristics and magnitude of the three subsystems of the UCS model have been studied and reported for the ABCP region, which will help to inform researchers and policymakers about the relationship between the local atmosphere and urban environment activities, specifically those related to pollutant emissions into the atmosphere.

## 2. Study area, data and methodology

### 2.1. Study area

ABCP, located in the MRSP southeast sub-region, is considered the largest industrial center of the MRSP, comprising seven municipalities: Mauá (MA), São Bernardo do Campo (SBC), Santo André (SA), São Caetano do Sul (SCS), Diadema (DIA), Ribeirão Pires (RP), and Rio Grande da Serra (RG) (Fig. 1). According to the Brazilian Institute of Geography and Statistics (IBGE, 2019), the ABCP region has 2,549,135 inhabitants, and part of its territory has high urban density with an intense population growth rate (56%); the other component contains environmental protection areas (Moro Junior, 2007). This spatial contrast results in different climate characteristics for the region. Moreover, ABCP was the first automobile industry center in Brazil. Currently, the service sector has been growing significantly and the region has a significant vehicles fleet. Table 1 summarizes the demographic characteristics of the ABCP municipalities.

With respect to hydrography, the Tamanduateí River, a tributary of the Tietê River, is the main watercourse in the urban area of ABCP, with a drainage area of 43 $km^2$. This area is heavily occupied with dense urbanization, a high industrial concentration, and little surface area for natural rainwater infiltration. Consequently, almost all the precipitation contributes to the Tamanduateí River channel and its tributaries, which receive rainwater runoff over the river's capacity and leads to flooding.

### 2.2. Data

This study used air temperature, relative humidity, wind speed, and direction hourly data (2010–2018) from 11 automatic weather stations (AWSs) managed by the São Paulo Flood Alert System and Santo André Municipal Environmental Sanitation Service. Daily rainfall data were obtained for the period 1999–2018 at the Department of Water and Electric Energy from 11 rain gauges distributed in the urban area of the ABCP region. Additionally, hourly $O_3$ and $PM_{10}$ data (from 1999 to 2018) provided by the Environmental Protection Agency (CETESB) from five air quality stations were used. Finally, data from two mixed deposition collectors were used for rainwater chemical analysis. The measurement stations are located throughout the urban areas of the study region (Fig. 1).

### 2.3. Methodology

Firstly, quality control of all the observed variables was performed, with the questionable and missing hourly and daily data being reviewed trough a consistency analysis. Then, the missing and inconsistent data were filled in using the Tabony (1983) Method, which uses a minimum of three neighboring stations for missing data calculation (Valero et al., 1996). For the identification of HI thermal characteristics, hourly air temperature data were used for diurnal cycle construction and, temperature differences (ΔT) were calculated between different meteorological station locations in the urban area (TU(h)); the station that is located most closely to an environmental preserved area (TR(h)) is also used as a rural reference area (Eq. (1)):

$$\Delta T_h = T_{Uh} - T_{Rh} \quad (1)$$

The ΔT value was categorized using the intensity classifications of Oke (1987) and Garcia (1996): weak (0 °C ≥ ΔT < 2 °C), medium (2 °C ≥ ΔT < 4 °C), and strong (4 °C ≥ ΔT < 6 °C). Negative values of ΔT are indicative of cooling islands.

The temperature and Humidity Index (THI) (Barbirato et al., 2007) and the Human Discomfort Index (HDI) (Ono and Kawamura, 1991) were used to estimate thermal comfort using the daily air temperature (T, °C), relative humidity (RH, %) and dew point temperature ($T_d$, °C). $T_d$ was calculated as a function of temperature and humidity. Eqs. (2) and (3) describe the indexes used. These indexes were developed for tropical regions and are suitable for outdoor environments. Table 2 presents the classification of THI and HDI values.

$$THI = 0.8 * T + \frac{RH * T}{500} \quad (2)$$

$$HDI = 0.99 * T + 0.36 * T_d + 41.5 \quad (3)$$

The assessment of the spatial similarity of daily rainfall patterns used cluster analysis based on Euclidean distances between points (Eq. (4)), which utilizes the distance between two points ($x_i$ and $x_j$) and notes dissimilarities between different variables (or groups). The criterion used to define the distance within the groups, which is associated with other groups, is based on the complete-linkage method, which tends to form more homogeneous and numerous groups (Wilks, 2006) once it takes into account the maximum difference. In this case, the largest Euclidean distance between a member of a G1 group and a member of a G2 group (Eq. (5)) is maintained. The separation process can be considered sufficient when there is a clear change in the distance between

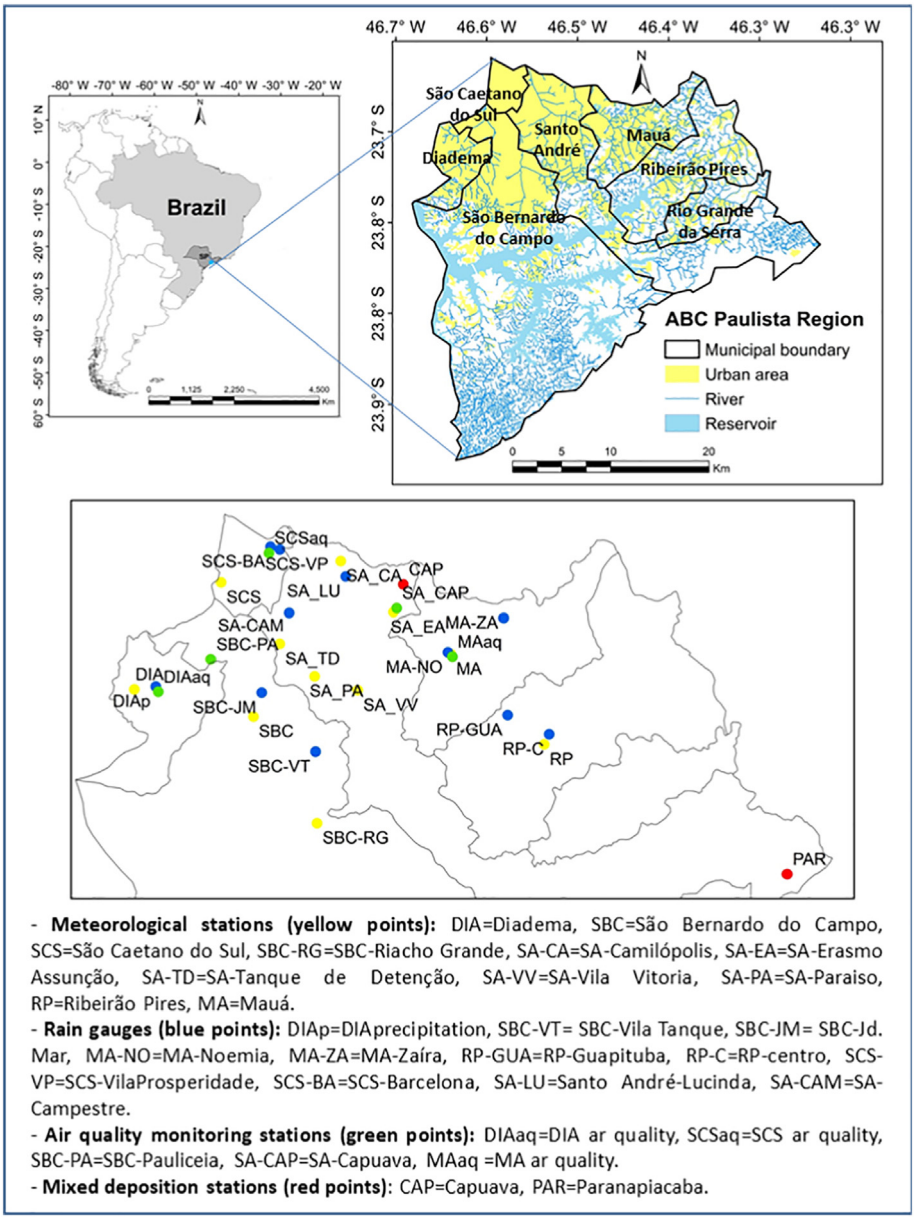


**Fig. 1.** ABC Paulista region in Brazil and location of atmospheric and air quality monitoring stations.

**Table 1**
Demographic and territorial characteristics of ABC Paulista municipalities.
Source: IBGE and Infrastructure and Environment Secretary of São Paulo State[a].

| Municipalities | Territorial area[b] ($km^2$) | Population[b] (inhabitants) | Demographic density[c] ($hab/km^2$) | Vegetation cover[d] (%) |
|---|---|---|---|---|
| Santo André | 175,782 | 716.109 | 3.848,01 | 35.78 |
| São Bernardo do Campo | 409,532 | 833.240 | 1.869,36 | 46.97 |
| São Caetano do Sul | 15,331 | 160.275 | 9.736,03 | 0.0 |
| Diadema | 30,732 | 420.934 | 12.536,99 | 4.81 |
| Mauá | 61,909 | 468.148 | 6.741,41 | 10.89 |
| Ribeirão Pires | 99,075 | 122.607 | 1.140,73 | 30.60 |
| Rio Grande da Serra | 36,341 | 50.241 | 1.210,04 | 56.68 |

[a] https://www.infraestruturameioambiente.sp.gov.br/sifesp/mapas-municipais/.
[b] Estimated value for 2018.
[c] 2010 Population Census.
[d] Regarding municipality area.

clusters, using the Pseudo-F statistic for determining the number of clusters. Each stage of the analysis compares the among-cluster sum of squares to the within-cluster, and a large Pseudo-F statistic (a peak) indicates distinct clusters.

The input parameters considered in the cluster analysis correspond to the geographic information (latitude, longitude, and altitude) of the studied stations and the daily precipitation indicators. The analysis considers only the rainy days, being that the precipitation indicators were

**Table 2**
Range values of THI (°C) and HDI indexes relative to thermal comfort condition.
Source: Barbirato et al. (2007), Ono and Kawamura (1991).

| THI | | HDI | |
|---|---|---|---|
| Comfortable | 21 < THI <24 | Heat stress | HDI > 80 |
| Slightly uncomfortable | 24 < THI <26 | Heat uncomfortable | 75 > HDI > 80 |
| Extremely uncomfortable | THI >26 | Comfortable | 60 > HDI > 75 |
| | | Cold uncomfortable | 55 > HDI > 60 |
| | | Cold stress | HDI < 55 |

created according to the mean of annual rainfall parameters, such as: mean daily rainfall, maximum daily rainfall, percentiles daily rainfall (95th, 85th, 65th, 35th and 15th), number of days with rain, and the mean and maximum value of the number of consecutive days with rainfall, both being discrete quantitative variables.

$$d_{ij} = \|x_i - x_j\| = \left[\sum_{k=1}^{K} (x_{i,k} - x_{j,k})^2\right]^{1/2} \quad (4)$$

$$d_{G_1,G_2} = \max_{i \in G_1, j \in G_2} \left|d_{ij}\right| \quad (5)$$

Hourly wind data were analyzed according to their intensity and predominant direction to identify the sea or land breeze phenomena, following Oliveira et al. (2003) for the breeze pattern in the MRSP. It is represented by a wind direction change from NE-NW to SE and enters São Paulo between 1:00 PM and 2:00 PM local time.

Analysis of atmospheric pollution in the ABCP region used information from fixed air quality stations and a transportation simulation model. $O_3$ and $PM_{10}$ levels were evaluated through an exploratory analysis that included identification of the diurnal cycle, seasonality, and number of days exceeding the air quality standards. The primary air quality standards for São Paulo correspond to $PM_{10}$ and are 120 μg $m^{-3}$ per 24 h and 40 μg $m^{-3}$ for an annual mean period; for $O_3$ it is 140 μg $m^{-3}$ per 8 h (CETESB, 2019).

The traffic simulation model used a transportation speed-sensitive emission calculation method. This model addresses the ABCP region as an open system because it is part of the MRSP, where a significant proportion of the emissions that occur in its territory are generated by pass-through traffic. The choice was based on the availability of the established and validated traffic model for the region developed by the São Paulo Metropolitan Trains Company (CPTM) in 2010 using the Equilibre Multimodal/Multimodal Equilibrium (EMME) software (Duarte and Paiva Junior, 2013). EMME generates traffic flow and speed results for a variety of planning scenarios and horizons. This work used data from the 2014 scenario that represents the current system of public and individual transport in the region as well as the system demand. EMME allocates MRSP's modeled travel matrix to the system peak hour that occurs between 7 and 8 AM. Thus, the results represent the system sections with the highest emission rates during the morning peak. The emission quantification was conducted to highlight the roads of interest in the region, so the study adopted the simplest national method (Table 3) that was also sensitive to EMME simulated traffic conditions (IPEA and ANTP, 1999; Duarte and Paiva Junior, 2013). The method of modeling emissions from mobile sources is based on road segments using a deterministic traffic simulation to generate the flow and velocity data required for the emission equations proposed by the Institute for Applied Economic Research – IPEA and National Public Transport Association – ANTP (IPEA and ANTP, 1999) in Table 3.

Analysis of mixed deposition (PM + rainwater) was performed at two sampling stations: the Paranapiacaba (PAR) district, a preserved area in SA with no direct impact from emission sources, and around the Capuava Petrochemical Complex (CAP), on the boundary of SA and MA, which characterized by the presence of industrial emissions and heavy-duty diesel-powered vehicles for cargo transportation. Mixed deposition samples from one week of exposure were collected in a manufactured device composed of a 20 L polyethylene bottle, protected with a 0.5 mm mesh screen to avoid contamination by external agents. Samples were collected from October 2016 to August 2017, a total of 25 sampling weeks. The pH and electrical conductivity of the mixed deposition samples were evaluated, and the major ionic composition was characterized using ion chromatography with conductivity detection (Vieira-Filho et al., 2015). Target analytes were inorganic species $Na^+$, $K^+$, $Ca^{2+}$, $Mg^{2+}$, $NH_4^+$, $F^-$, $Cl^-$, $NO_3^-$, and $SO_4^{2-}$. An aliquot of rainwater samples was separated and acidified with 2 mL of concentrated $HNO_3$ for analysis of lead and cadmium concentrations by inductively coupled plasma optical emission spectrometry (Chubaka et al., 2018).

Principal component analysis (PCA) was performed to evaluate the interrelationships between analyzed variables, in order to explain them in terms of their inherent dimensions (components). PCA is considered the optimal linear transformation, and the number of major components becomes the number of variables considered in the analysis, but generally the first components are the most important as they explain most of the total variation (Wilks, 2006). PCA finds eigenvalues (variance) of a sample covariance matrix and eigenvectors (weights) within this result to perform dimensional reduction of the data and analyze the main patterns of variability present. Detailed PCA formulations can be found in Wilks (2006).

## 3. Results and discussion

Air temperature, relative humidity, and precipitation mean seasonal cycles in the urban area of ABCP are shown in Fig. 2. Temperature and relative humidity analysis correspond to the period of 2015–2018 for the five municipalities evaluated. This period was selected, since there are data available for all municipalities. Precipitation data correspond to the period 1999–2018. Fig. 2a shows the annual cycle and identifies a well-defined seasonality with the warmest and wettest months from November to March. The summer presented the highest temperatures (~22.9 °C) and rainfall (~200.1 mm). The month with the least amount

**Table 3**
IPEA/ANTP emission equations.

| Light vehicles (Emissions in g $km^{-1}$) | Heavy vehicles (Emissions in g $km^{-1}$) |
|---|---|
| $HC = -0.28 + \frac{62.48}{V}$ | $\begin{cases} \text{Se } V<32.44\text{km/h} \rightarrow HC = 14.14 - 3.67 \cdot \ln V \\ \text{Se } V \geq 32.44\text{km/h} \rightarrow HC = (-0.55518 + \frac{62.48}{V}) \end{cases}$ |
| $CO = -4.51 + \frac{727}{V} + 0.00134 \cdot V^2$ | $CO = 43.34 - 8.98 \cdot \ln V$ |
| $NO_x = 1.03 + 0.00007477 \cdot V^2$ | $NO_x = 37.21 - 6.46 \cdot \ln V$ |
| $SO_x = 0.16$ | $\begin{cases} \text{Se } V<22\text{km/h} \rightarrow SO_x = 2.2770 - 0.3971 \cdot \ln V \\ \text{Se } V \geq 22\text{km/h} \rightarrow SO_x = 1.6639 - 0.3971 \cdot \ln V \end{cases}$ |
| $MP = 0.08$ | $MP = 1.7359 - 0.3186 \cdot \ln V$ |
| $CO_2 = 8{,}888.2 \cdot V^{-0.986}$ | $CO_2 = 4{,}067.2 \cdot V^{-0.396}$ |
| V – speed (km $h^{-1}$) | MP – emission rate of particulate matter (g $km^{-1}$) |
| HC – hydrocarbon emission rate (g $km^{-1}$) | $CO_2$ – carbon dioxide emission rate (g $km^{-1}$) |
| CO – carbon monoxide emission rate (g $km^{-1}$) | |
| NOx – nitrogen oxide emission rate (g $km^{-1}$) | |
| SOx – sulfur oxide emission rate (g $km^{-1}$) | |

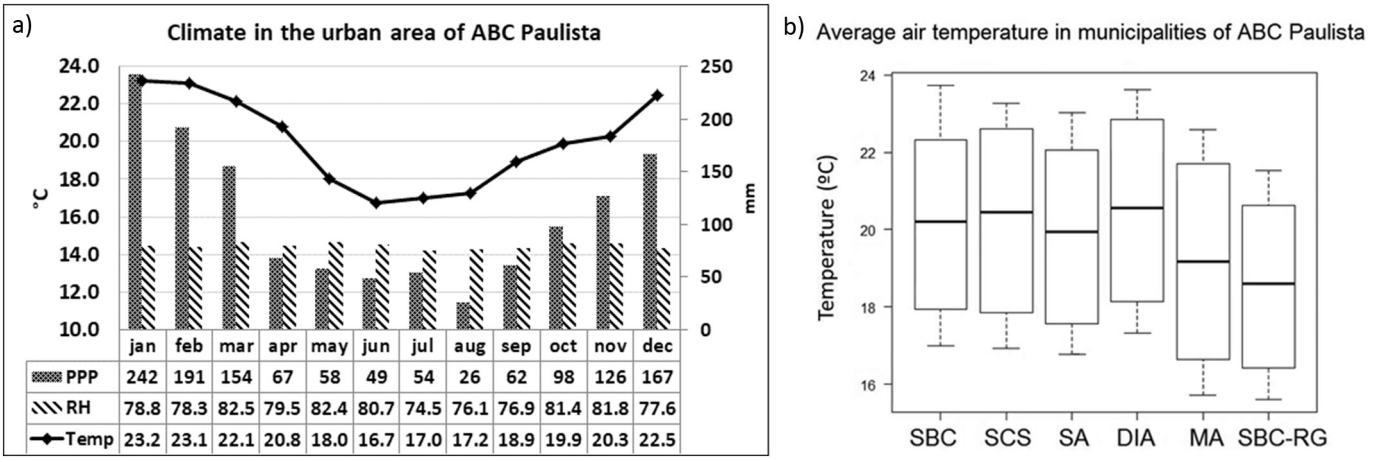


**Fig. 2.** Annual cycle of mean air temperature, relative humidity (RH) and precipitation (PPP) for the urban area of ABC Paulista (a), and the annual cycle of temperature in each municipality of ABC Paulista for the period 2015–2018 (b).

of rainfall is August, and the month with the lowest temperature is June. The relative humidity is highest in autumn and spring.

Fig. 2b shows the monthly average temperatures for each of the analyzed AWSs (Table 1). The Riacho Grande AWS in São Bernardo do Campo (SBC-RG) was used as a rural area reference station, as it is located in a neighborhood with an environmental preservation area and the Billings Dam. SA has five AWSs; thus, the study calculated a value representing the average temperature of the urban area for the municipality.

The average monthly temperatures of DIA, SCS, and SBC have similar median values, and in DIA and SCS the temperature are slightly higher in the summer. The municipalities of DIA and SCS have the highest demographic density, lowest vegetation cover and smallest territorial area (Table 1). This suggests greater impermeable surfaces from buildings construction and consequently, a greater anthropogenic heat source that influences the temperature increase and humidity reduction.

The lowest temperature values were found in SBC-RG because it is far from the dense urban area. The largest temperature difference in the urban area when compared to the SBC-RG station was in February for the municipalities of SBC (3.2 °C), DIA (3.0 °C), and SCS (2.7 °C).

### 3.1. Urban Heat Islands

For HI intensity calculation (ΔT), the average monthly diurnal air temperature cycle of each AWS was constructed, and the SBC-RG AWS was the rural reference location. Performing calculations throughout the diurnal cycle identified the most intense daytime ΔT. To summarize the results, the ABC urban region was divided by sub-regions according to geographic location, and this calculation considered the five AWSs of the SA municipality (SA-CA, SA-EA, SA-TD, SA-PA, and SA-VV) (Fig. 1). Table 4 shows the monthly average ΔT for each region for the 2015–2018 period. The values of ΔT (Table 4) identified the Northwest ABC (municipality of DIA) as the warmest sub-region, characterizing a heat island of medium intensity according to the classification of Oke (1987). The ΔT values are more intense in spring and summer, with a highest value of 3.7 °C in October. The maximum values were found in the afternoon, most frequently in the period between 3:00 PM and 5:00 PM. The second warmest region corresponds to the northern part of ABCP, comprising the municipality of SCS and part of SA.

Fig. 3(a) shows the average temperature spatialization for January at 4:00 PM, performed through the Kriging interpolation method from the ArcGIS10.3.1 software, which was conducted in an area with more AWS data. Warmer areas are located preferably on the northwest region of ABCP, in the municipalities of DIA (north and northwest region), SCS, and the north and northwest of the urban area of SA and SBC in agreement with the ΔT. The coldest areas are in the south and east of the urban area. Fig. 3(b) shows the diurnal cycle for the same month between the DIA and SBC-RG stations, with the highest ΔT value being 3.2 °C.

### 3.2. Thermal comfort

Thermal comfort was evaluated by the THI and HDI indices on daily and monthly scales between 2:00 PM and 4:00 PM, when the HI intensity was at a maximum. Fig. 4(a) shows the results for the THI, with the lower and upper limits delimiting the slightly uncomfortable zone (Table 2), in which all the analyzed municipalities in the summer months (January and February) presented higher THI values, while they only showed the same pattern for some months in autumn (March and April) and spring (September and November).

Instead, the municipalities of DIA, SCS and SBC stand out with THI values above the upper limit (>26 °C), especially in the summer, which indicates an extremely uncomfortable situation (Table 2). In

**Table 4**
The intensity of atmospheric urban heat island obtained by diurnal cycle ΔT (°C) for the 2015–2018 period.

| ABCP region | Summer | | | Autumn | | | Winter | | | Spring | | |
|---|---|---|---|---|---|---|---|---|---|---|---|---|
| | Dec | Jan | Feb | Mar | Apr | May | Jun | Jul | Aug | Sep | Oct | Nov |
| North (SCS, SA-CA, SA-EA SA-TD) | 2.7 | 2.6 | 2.7 | 2.5 | 2.1 | 2.1 | 2.4 | 2.3 | 2.5 | 2.6 | 2.8 | 2.5 |
| Center (SBC, SA-VV e SA-PA) | 2.3 | 2.8 | 2.6 | 1.7 | 1.7 | 1.7 | 1.9 | 1.8 | 2.1 | 2.0 | 2,1 | 2.1 |
| Northeast (MA e RP) | 2.3 | 2.2 | 1.4 | 1.3 | 1.3 | 1.3 | 1.6 | 1.4 | 1.6 | 1.4 | 1,5 | 1.4 |
| Northwest (DIA) | 3.1 | 3.2 | 2.9 | 2.9 | 2.6 | 2.5 | 2.8 | 2.8 | 3.0 | 3.2 | 3.7 | 3.1 |

Low magnitude heat island (>0 °C ΔT < 2,0 °C).
Medium magnitude heat island (≥2,1 °C ΔT < 4,0 °C).

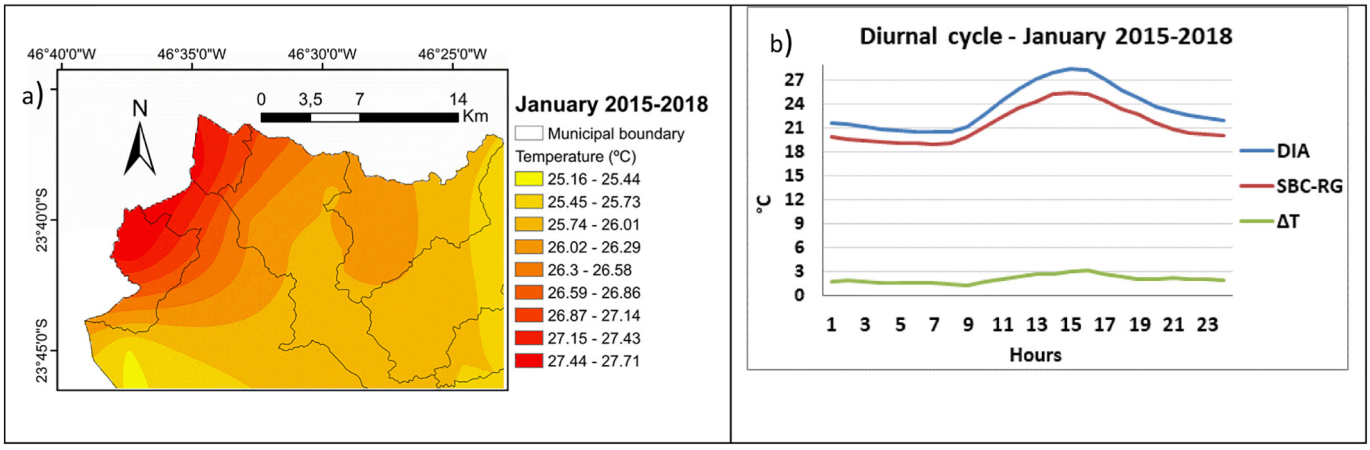


**Fig. 3.** The spatialization of air temperature for January (2015–2018) (a) and diurnal cycle of temperature for January (2015–2018) (b).

2015, one of the warmest years in the last decade according to the World Meteorological Organization (WMO, 2019), almost all municipalities experienced extremely uncomfortable thermal comfort levels, except for Riacho Grande in SBC. In year 2015, DIA, SCS and MA were the municipalities that reached the highest THI values, which are associated with an extremely uncomfortable situation.

According to the HDI (Fig. 4b), all municipalities presented values within the "uncomfortable due to heat" level (Table 2), as identified by the upper and lower limits. Unlike THI, in 2015, the HDI did not show values above the upper limit, but the values for the municipalities of DIA, MA, SCS and SBC were the highest in January in 2015.

Despite the higher intensity of HIs had been in October, it was verified that the indices identified uncomfortable condition mostly in the summer months due to higher air temperatures; however, this does not mean that, on specific days of spring, or any other season, no days of extreme discomfort were recorded, since the calculation of these

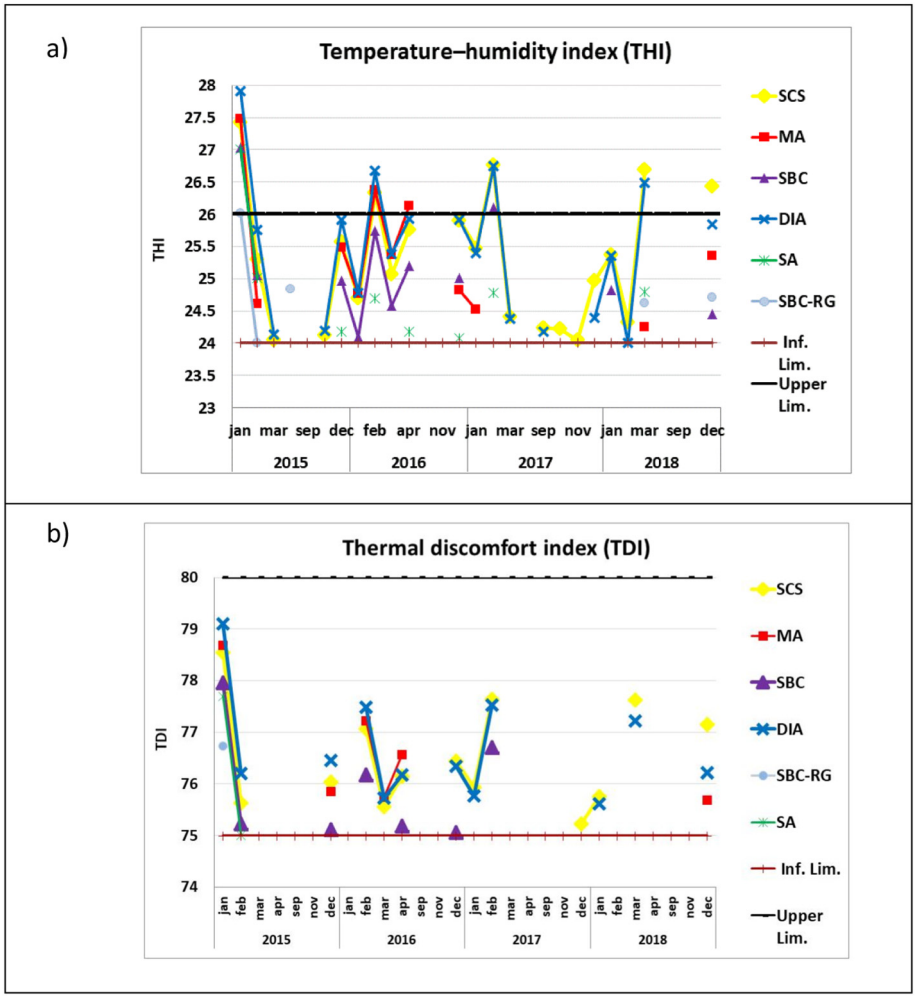


**Fig. 4.** Temperature-humidity index (a) and thermal discomfort index (b) for the ABC Paulista municipalities.

indices is directly related to humidity and synoptic profiles. On wetter days, heat loss through evaporation is reduced, so warmer and wetter days usually cause greater discomfort to the population compared to hot and dry days (Nóbrega and Lemos, 2011).

### 3.3. Identification of the predominant local circulation

The analysis of wind direction and intensity for each AWS located in the municipalities identified the predominant types of wind associated with the sea and land breezes: the standard breeze, a wind with a northeasterly component (NE) in the morning, turning southeasterly (SE) in the afternoon (SB_1); a northwesterly wind (NW) in the morning becoming SE in the afternoon (SB_2); and a breeze with a SE component in the daytime (morning and afternoon). In addition, the wind was predominantly W-NW in the afternoon and *E*-SE in the morning, suggesting an inverted breeze pattern called a terrestrial breeze (TB). Another type of movement identified was NE-E winds in the morning and SW-W winds in the afternoon, which is referred to as SB_3. Some AWSs showed a large amount of variability in wind direction over the analyzed period (2015–2018) and were classified as having variable winds (VW) with an undefined pattern.

Wind direction analysis was performed daily and divided into four periods (1:00–6:00 AM, 7:00 AM -12:00 PM, 1:00–6:00 PM and 7:00 PM -12:00 AM). Table 5 presents the results for each municipality and corresponds to the morning (7:00 AM -12:00 PM) and afternoon (1:00–6:00 PM) periods. The number between parentheses represents the average percentage of days for each month with the characteristic pattern. The other days had a large amount of variability that could indicate any other type of pattern for specific weather conditions or even no breeze pattern.

In DIA, with the highest HI intensity and hottest temperatures, there was a TB pattern in almost every month of the year that was more frequent during autumn days. This pattern is characterized by W-NW afternoon winds, receiving the warmest and driest winds from the most waterproofed areas coming from the center of the MRSP, which contributes to the temperature increase. Even in some spring months, W-NW winds prevail during the day.

In SCS, the municipality rated as the second hottest, a typical sea breeze pattern was observed in almost every month of the year, with a higher percentage (≥50%) in autumn and December. Only in January and February do *E*-SE winds prevail during the day.

Although sea breezes are known to minimize the HI intensity, other factors may influence the temperature intensity, such as a higher population density, excessive construction of buildings, and low concentration of green areas in the ABCP region, which contribute to temperature increases. Concrete, asphalt and other materials that are typical of urban centers have higher emissivity values than vegetation does, allowing for an increase in temperature (Freitas et al., 2007).

SBC municipality primarily had SB_2 winds, with NW wind in the morning turning to the SE in the afternoon. This pattern type showed a higher percentage of days in the summer and spring months (≥50%).

In the municipality of MA, there was a predominance of the SB_3 pattern: winds in the morning with a NE-E direction and those in the afternoon with a SW-W direction. The AWS in this municipality is located in the northeastern of ABCP, which has more rugged topography, so the SW-W winds in the afternoon may be influenced by the landscape. The topography and vegetation coverage influences the winds circulation; mountains and valleys channel the breeze, and also provide a favorable environment for its formation. Different types and levels of vegetation coverage may also encourage faster temperature increases, which can initiate the breeze circulation (Atkinson, 1981). MA has fewer impermeable areas with greater vegetation cover and very irregular topography compared to urban areas from other municipalities (Table 1). Since the analysis is conducted on a daily basis, synoptic or mesoscale systems can also influence the wind direction.

The SA winds had an SB_2 pattern in the summer months and an SB_1 pattern in autumn, winter, and early spring. In the SBC-RG station, the standard breeze circulation (SB_1) was identified preferentially for the autumn, winter, and spring months. In January and February, there were winds from the E-SE during the day, so it was possible to verify that the sea breeze was managing to maintain milder air temperatures; this location is also less urbanized and close to the Billings Dam area.

Fig. 5 shows the average diurnal cycle for the ABCP region and the wind speed for each season of the year. On average, the highest wind intensities (1.9 m $s^{-1}$) occurred from 2:00 PM to 4:00 PM. The seasonal wind speed for each municipality shows that the highest wind intensity occurred in spring and summer. In the DIA and SCS municipalities, where air temperatures are higher, the wind intensity was lower, especially in SCS. Usually, in denser and more vertically developed areas, the wind intensity tends to be lower due to the surface roughness, which also contributes to controlling the attenuation of the HI. SBC-RG also had lower wind intensities, likely due to the location being closer to

**Table 5**
Wind circulation pattern - breeze types. The percentage values meaning the average percentage of days for each month with a type of wind pattern.

| City | Summer | | | Autumn | | | Winter | | | Spring | | |
|---|---|---|---|---|---|---|---|---|---|---|---|---|
| | Dec | Jan | Feb | Mar | Apr | May | Jun | Jul | Aug | Sep | Oct | Nov |
| DIA | TB (30%) | TB (34%) | W-NW (35%) | TB (45%) | TB (40%) | TB (35%) | TB (39%) | TB (34%) | W-NW (25%) | VW | W-NW (25%) | W-NW (45%) |
| MA | SB_3 (30%) | SB_3 (30%) | SB_3 (20%) | SB_3 (25%) | VW | VW | SB_3 (25%) | SB_3 (28%) | SB_3 (20%) | SB_3 (28%) | SB_3 (25%) | SB_3 (20%) |
| SBC | SB_2 (50%) | SB_2 (50%) | SB_2 (52%) | SB_2 (40%) | *E*-SE (50%) | SB_2 (40%) | SB_2 (40%) | SB_2 (50%) | SB_2 (52%) | SB_2 (50%) | E-SE (40%) | E-SE (40%) |
| SBC–RG | SE-S (28%) | SB_1 (20%) | SB_1 (20%) | SE-S (30%) | SE-S (30%) | SE-S (30%) | SB_1 (35%) | SB_1 (20%) | SE-S (30%) | SE-S (35%) | SE-S (33%) | SE-S (35%) |
| SA | SB_2 (46%) | SB_2 (43%) | SB_2 (40%) | SB_1 (45%) | SB_1 (34%) | SB_1 (36%) | SB_1 (42%) | SB_1 (38%) | SB_1 (53%) | SB_2 (53%) | SE-S (50%) | SB_2 (39%) |
| SCS | E-SE (30%) | E-SE (30%) | SB_1 (50%) | SB_1 (50%) | SB_1 (55%) | SB_1 (40%) | E-SE (40%) | SB_1 (40%) | SB_1 (45%) | SB_1 (40%) | SB_1 (35%) | SB_1 (56%) |
| Standard breeze | | | Code | | | Morning | | | Afternoon | | | |
| | | | SB_1 | | | NE (North East) | | | SE (South East) | | | |
| | | | SB_2 | | | NW (North West) | | | SE | | | |
| | | | SB_3 | | | NE-E (North East – East) | | | SW-W (South West – West) | | | |
| Terrestrial breeze | | | TB | | | E-SE (East - South East) | | | W-NW (West - North West) | | | |
| Variable wind | | | VW | | | Undefined pattern | | | | | | |
| Others | | | SE-S | | | South East – South (Morning and Afternoon) | | | | | | |
| | | | E-SE | | | Morning and Afternoon | | | | | | |
| | | | W-NW | | | Morning and Afternoon | | | | | | |

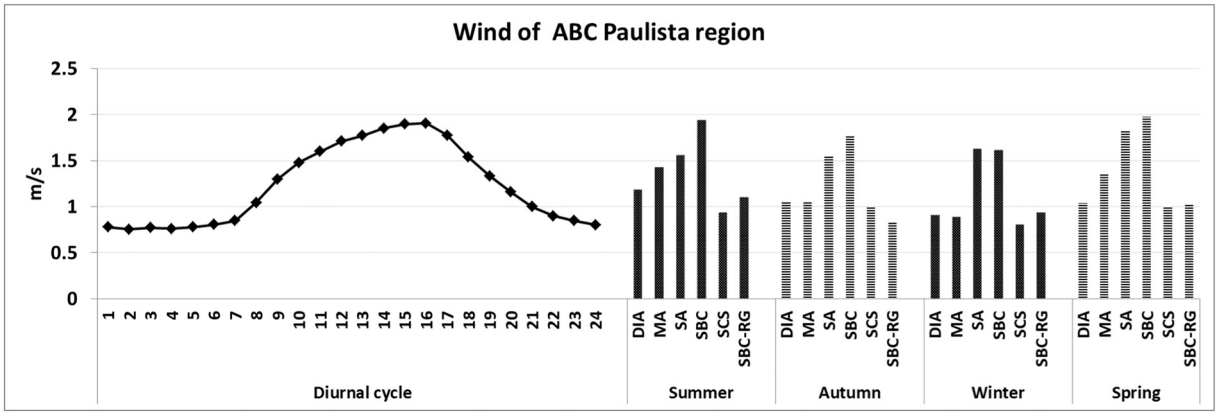


**Fig. 5.** Diurnal cycle of wind speed for ABC Paulista region and mean speed per seasons for the period 2015–2018.

an environmental preservation area and due to vegetation roughness. SBC and SA had the highest wind intensities.

### 3.4. Identification of areas with higher frequencies of extreme rain events

The hierarchical cluster analysis based on Euclidean distances identified five groups with distinct characteristics (Fig. 6). As in most municipalities (except for DIA), there is more than one rain gauge, so different patterns were verified between stations within the same municipality (except for SCS), and similar patterns were identified between stations in different municipalities.

Group 1 (G1) includes RP-Guapituba (RP-GUA: cyan colored station in Fig. 6) and presents the most distinct pattern of daily precipitation, the greatest number of days with rain, and a higher number of consecutive days with rain compared to other stations. Also, the lower percentiles daily rainfall (15th and 35th) presented the highest values.

The second group (G2) consists of two stations in different municipalities (SA – CAM and DIA, in pink in Fig. 6). This group stands out for its higher values of the mean and maximum daily precipitation related to extreme precipitation thresholds (85th and 95th percentiles); however, they have lower numbers of days with rain and consecutive days with rain, which indicates concentrated and intense rainfall in these locations, especially at DIA.

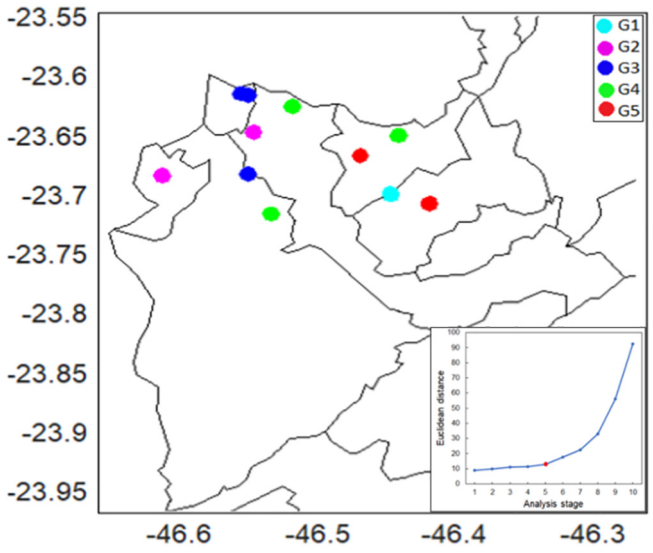


**Fig. 6.** Map indicating the precipitation station groups formed by cluster analysis, highlighting the location of each group member. In the right base, the Euclidean distance is highlighted by the stage of analysis and the jump point (in red). (For interpretation of the references to colour in this figure legend, the reader is referred to the web version of this article.)

The rain gauges of SCS (SCS-BA and SCS-VP) were grouped with the northern station of SBC-JM in the third group (G3). These locations have similar altitudes and intermediate characteristics in terms of the number of days with rain, mean total, and extreme daily rainfall; however, the SCS-VP (east of SCS) had a greater number of rainy days than did others in the group.

Group 4 (G4, green in Fig. 7) includes rain gauges from three distinct municipalities, SBC-VT, SA-LU, and MA-ZA, and presents the intermediate daily rainfall in terms of annual mean and percentiles. The major differences, however, are in the group's locations at higher altitudes and differences in their land use and occupations, as in Zaíra and Vila do Tanque (Neighborhood Montanhão), which are characterized by precarious housing and increase the population's vulnerability to the impacts of heavy rainfall.

The last group (G5, red in Fig. 7), which includes the rain gauges of Ribeirão Pires (RP-C, central region) and MA-NO, has a lower daily mean rainfall compared to that of the previous groups. Specifically, for RP-C, the total daily precipitation, percentiles analyzed, number of days with rain, and consecutive days with rain are lower than those of other rain gauge in the same municipality (RP-GUA). The rain gauges of this group are located in dense areas and, have similar altitudes (lower than the neighborhood), and geographical proximity that may contribute to the grouping process.

Regarding the impacts of daily rainfall on ABCP, along with the increase in daily rainfall over a short period of time, the occurrence of floods or mass movements also relates to the vulnerabilities from each ABCP municipality. According to Valverde (2017), the municipalities of DIA and MA are the most vulnerable to intense rainfall and its impacts, because they present increasing trends in the number of days with moderate rainfalls events (≥50 mm) and are conditioned by demographic, socioeconomic, and sanitation determinants. These determinants influence the municipality's ability to respond, recover, or adapt to the threats of heavy rain. Historical records for the period 2012–2014 showed that landslide events are more frequent than floods (except in SCS), with the highest frequency of floods occurring in SA and MA (Valverde et al., 2018).

### 3.5. Analysis of air pollution in ABCP

#### 3.5.1. Stationary sources in monitoring stations

The pollutants $O_3$ and $PM_{10}$ were selected for analysis as they are monitored by CETESB in almost all municipalities of ABCP. These pollutants, especially the $PM_{10}$, are relevant for health conditions, and $O_3$ showed an upward trend mainly due to vehicular emissions of $NO_x$ and VOCs in the MRSP (Alvim et al., 2018; Andrade et al., 2017).

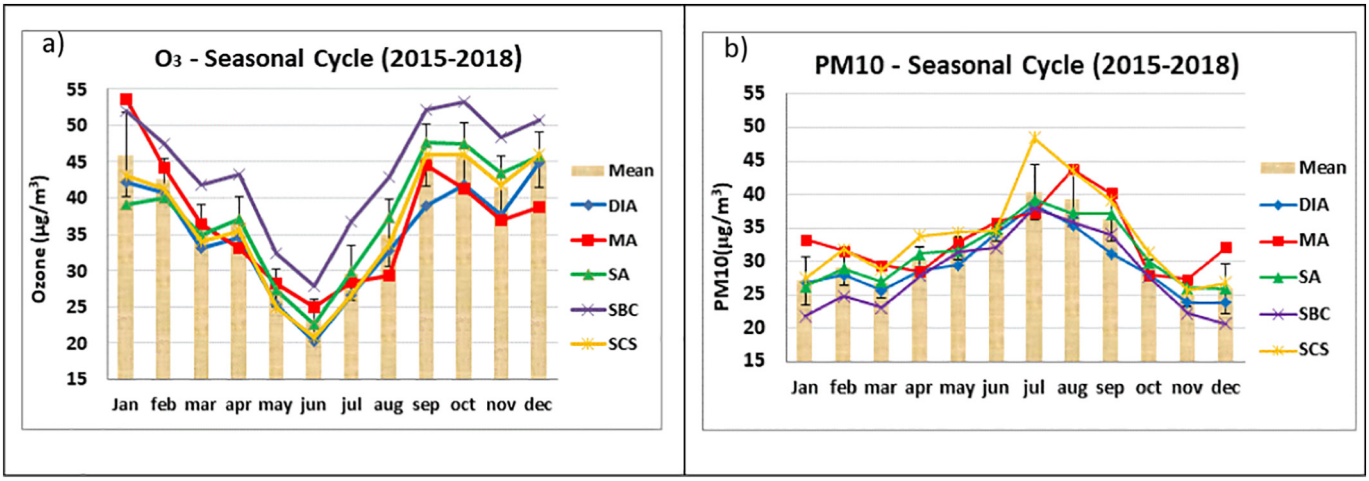


**Fig. 7.** Seasonal cycle of Ozone (a) and Particulate Material ($PM_{10}$) for 2015–2018 period.

Fig. 7 shows the average seasonal cycle of the $O_3$ and $PM_{10}$ concentrations for 2015–2018. Ozone concentrations are higher in the spring and summer months (Fig. 7a), and the municipality of SBC presented the highest concentration values in almost every month, especially in spring, with an average value of 52.1 μg $m^{-3}$ in October. Conversaly, MA had the highest value in January (53.6 μg $m^{-3}$), followed by SBC (52.0 μg $m^{-3}$). Ozone production is facilitated on sunny and warm days during the spring and summer. $O_3$ is also considered a greenhouse gas and a toxic air pollutant, with serious implications for climate, human health, and agricultural productivity (IPCC, 2007; Alvim et al., 2018).

The seasonal cycle of $PM_{10}$ concentrations (Fig. 7b) had the highest values from July to September and the lowest values in the summer months. The municipality of SCS presented the highest concentrations between July (48.5 μg $m^{-3}$) and August (43.6 μg $m^{-3}$), and MA had the highest concentrations between August (43.8 μg $m^{-3}$) and September (40.2 μg $m^{-3}$).

Higher $PM_{10}$ concentrations are associated with weather conditions that do not favor dispersion. An unfavorable condition is the absence of rain, and in the MRSP, the July–September period is characterized by a dry season with little rainfall volume, making wet removal difficult (CETESB, 2019). During the July–September period, the South Atlantic Anticyclone is closer to the Brazilian southeast coast, causing stable conditions and contributing to low levels of dispersion. Soft winds or stable atmospheric conditions also prevent the dispersion of pollutants.

On the other hand, urban factors also influence the dispersion of pollutants. According to Deryugina et al. (2019) the direction and position of main highways and factories can also lead to the advection of pollution depending on the wind direction.

The average diurnal ozone cycle (Fig. 8a) indicated that the highest values occur in the period from 1:00 PM – 3:00 PM, with the highest incidence of radiation to the surface. The city of SBC had the highest values and had an $O_3$ value of 83.6 μg $m^{-3}$ at 2:00 PM. SCS had the second highest value (78.4 μg $m^{-3}$) at 3:00 PM.

$PM_{10}$ concentrations were greatest in the first few hours of the day (1:00 AM–3:00 AM), with DIA (53.2 μg $m^{-3}$) and SA (53.3 μg $m^{-3}$) demonstrating the highest values. In addition, another secondary peak between 4:00 PM–6:00 PM was observed, and SBC (46.4 μg $m^{-3}$) had the highest concentration at 5:00 PM. The municipality of SA presented the lowest concentrations during the period from 4:00 AM–2:00 PM.

One of the explanations for the high concentrations during the early morning hours is related to the nocturnal boundary layer that forms at low altitudes (<300 m), creating a thermal inversion that is characteristic of a stable atmosphere. The pollutants are confined within a thin volume of air, contributing to high concentrations during the early morning (Castanho, 1999).

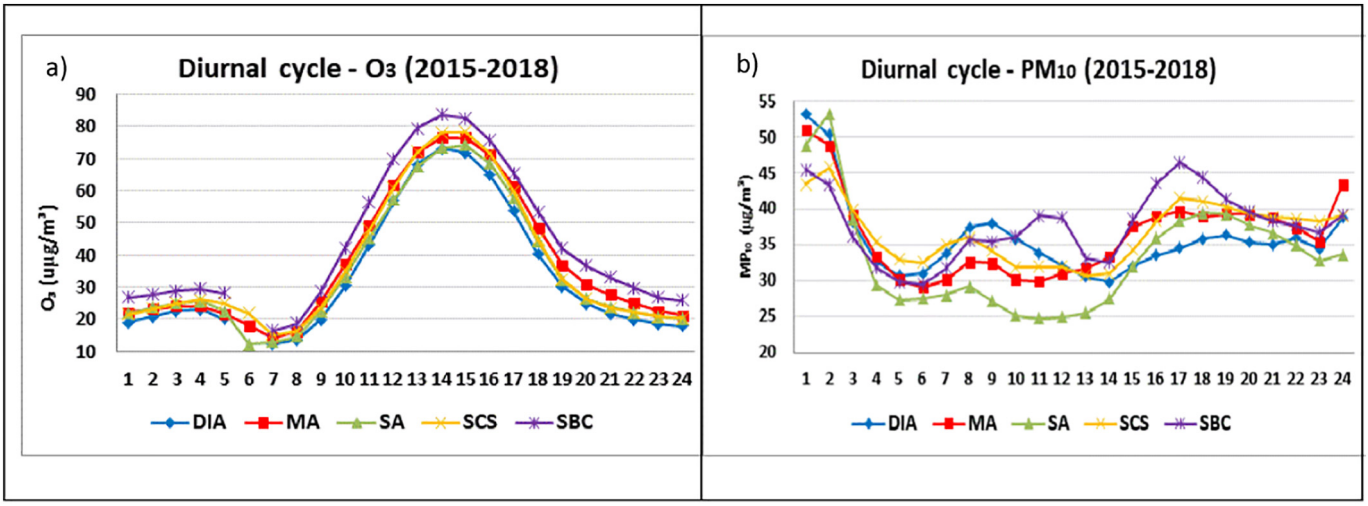


**Fig. 8.** Diurnal cycle of $O_3$ (a) and $PM_{10}$ (b) for 2015–2018 period.

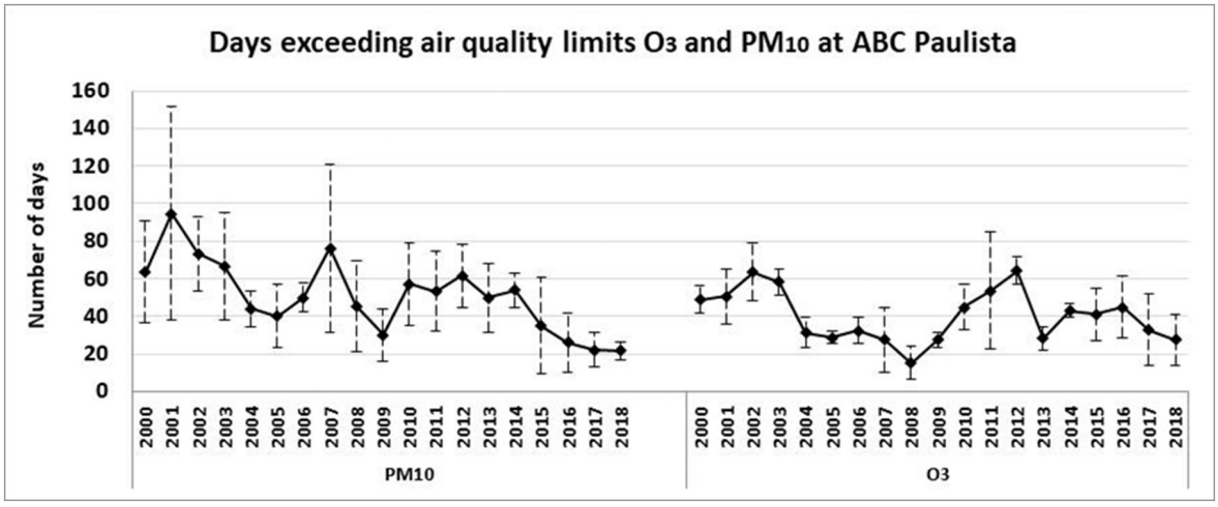


**Fig. 9.** Number of days exceeding air quality standard for $PM_{10}$ and $O_3$ in the period 2000–2018 for ABC Paulista. These values represent the mean values among the municipalities considered. The bars show the standard deviation of the number of days among the municipalities.

Fig. 9 shows the number of days in which $O_3$ and $PM_{10}$ concentrations exceeded air quality standards over the period 2000–2018. The number represents an average value for the ABCP region considering the municipalities of SA, SBC, SCS, DIA, and MA. The bars represent the standard deviation of values between municipalities.

$PM_{10}$ displays a decreasing trend in the number of days exceeding of air quality standards. In some specific years, higher standard deviations were observed, meaning there were large differences in values between municipalities; for example, in 2001, DIA presented a high value of 191 days, and in 2007, SBC had 153 days exceeding the limit. The years 2003 and 2015 also showed high values of deviation, with MA (108 days) and SCS (78 days) standing out relative to the other municipalities.

According to CETESB, the average annual value of $PM_{10}$ has a quality standard limit of 40 μg $m^{-3}$. This study verified that all the analyzed municipalities presented annual average values above the limit during 1998 to 2002. After these years, there was a decreasing trend, and eventually the limit was exceeded again in the municipalities of MA (2007, 2010, and 2014) and SBC (2007 and 2010).

The transportation sector is the main industry responsible for pollutant emissions, including $PM_{10}$. Thus, it was necessary to establish laws for the reduction of emissions, such as CONAMA Resolution No. 18 and the Motor Vehicle Air Pollution Control Program (PROCONVE). These programs set the first emission limits for light vehicles and contributed to meeting established air quality standards. On October 28, 1993, Law No. 8723 enforced the requirement to reduce emission levels of air pollutants. Thus, PROCONVE was implemented in phases and became the main factor reducing air quality violations in Brazilian cities through an applicable law to reduce pollutants, promote the large-scale use of biofuels such as ethanol and biodiesel, and reduce sulfur content in fuels (Andrade et al., 2017).

Ozone did not show a clear decreasing trend because for the period 2002–2008, there was a decrease that was subsequently followed by an increase until 2012 (Fig. 9). In analyzing the individual behavior for each municipality of ABCP, some showed slight decreases, such as MA and DIA, but others presented a slight increase, such as SCS and SA. The year 2011 stood out for presenting very high standard deviations due to SCS exceeding the limit in 100 days; however, in 2012, all municipalities had higher values that were closer in magnitude that ranged from 55 (DIA) to 71 days (MA). Considering only the period 2015–2018, the SCS municipality had the largest number of days exceeding $PM_{10}$ levels (173), followed by MA. On the other hand, SBC exceeded the limit of $O_3$ for the highest number of days (217), followed by SCS (176).

Ozone and $PM_{10}$ are short-lived climate pollutants (UNEP, 2011), and anthropogenic heat sources for the temperature increase. Thus, the high concentrations of pollutants in SCS and SBC may also be associated with the characteristic of warmer municipalities and with the formation of HIs.

*3.5.2. Identification of roads and transport corridors with the highest vehicular emissions potential in ABCP*

The traffic simulation model used to identify the highest emission roads and corridors made it possible to obtain information on other pollutants and greenhouse gases, such as: $CO_2$, CO, $NO_x$, $SO_x$, HC, and PM in the 2014 scenario. Despite the scenario time lag, it is probably the closest to the current state of the transportation system, considering the economic downturn, lack of infrastructure improvements, and impacts that new projects will have on ABCP in the near future.

In the MRSP, air quality problems are generally associated with vehicular emissions. For example, tropospheric $O_3$ is produced from the photochemical oxidation of vehicle emission pollutants, accounting for approximately 97%, 79%, 67%, 17%, and 40% of CO, HC, $NO_x$, $SO_x$ and PM emissions, respectively (CETESB, 2016; Andrade et al., 2017).

The transportation model results show the calculation of emissions by each CPTM macrosimulation network model segment and provide the vehicle flow by fleet type and average traffic speed in every link or segment of the network during the morning peak (7:00–8:00 AM). The fleet considered automobiles to be light vehicles and municipal and metropolitan buses as well as heavy-duty vehicles (trucks) to be heavy vehicles.

Table 6 shows the emissions in kg $km^{-1}$ of pollutants for the municipalities of ABCP. Concerning the total mass of emissions in kg $km^{-1}$, SCS and SBC stand out with large total emissions values. In SCS, the CO, $CO_2$, and HC emissions have the highest values, especially $CO_2$ with a mass of 649.08 kg $km^{-1}$, compared to those of other cities. In SBC, pollutants $SO_x$ (0.23 kg $km^{-1}$) and PM (0.16 kg $km^{-1}$) increase with greater mass. On the other hand, MA was the second municipality with the highest CO and HC masses.

Fig. 10 shows maps with road segments of the traffic model, highlighted in red according to the magnitude of their emissions. Fig. 10a shows $CO_2$ emissions, and red bar thicknesses indicate the intensity of $CO_2$ emissions per km in the model sections. It can be seen that the thicker stretches are more evident in the large avenues of the study region, on DIA city, the north-western stretch of Imigrantes Highway (1), MA at Papa João XXIII Avenue (2), and Dos Estados Avenue that connects the SA city center to the north of SCS (3), for example.

**Table 6**
Emissions in kg km$^{-1}$ road by city of ABC Paulista (peak hour 7 h–8 h), for each chemical compound and particle.

| City | Total mass (kg) | Total mass | CO | $CO_2$ | NOx | SOx | HC | PM |
|---|---|---|---|---|---|---|---|---|
| | | kg km$^{-1}$ road | kg km$^{-1}$ road | kg km$^{-1}$ road | kg km$^{-1}$ road | kg km$^{-1}$ road | kg km$^{-1}$ road | kg km$^{-1}$ road |
| SBC | 390,154.93 | 630.87 | 35.91 | 588.64 | 2.39 | 0.23 | 3.00 | 0.16 |
| SA | 235,672.84 | 445.91 | 28.93 | 413.24 | 1.02 | 0.13 | 2.52 | 0.07 |
| MA | 120,499.36 | 608.37 | 39.73 | 563.62 | 1.31 | 0.16 | 3.46 | 0.09 |
| DIA | 93,100.84 | 415.98 | 25.70 | 386.47 | 1.38 | 0.15 | 2.21 | 0.09 |
| SCS | 85,481.15 | 700.44 | 45.64 | 649.08 | 1.45 | 0.17 | 4.01 | 0.09 |
| RP | 55,600.95 | 457.77 | 23.54 | 429.06 | 2.95 | 0.20 | 1.87 | 0.15 |
| RGS | 2,219.95 | 57.47 | 3.38 | 53.43 | 0.34 | 0.04 | 0.26 | 0.02 |
| Total | 982,730.03 | 530.94 | 32.24 | 493.78 | 1.88 | 0.17 | 2.75 | 0.11 |

$NO_x$ emissions by road links are shown in Fig. 10b. The thicker stretches are along the major roads that cross the cities, such as Imigrantes Highway, which crosses DIA city from its southeastern to northwestern (1) regions. In addition, other major stretches are found on the Anchieta motorway (4) that crosses from south to north SBC; however, the road that stands out the most is Rodoanel Mário Covas Orbital Motorway (5), crossing SBC, SA, and RP. The spatial arrangement of PM is quite similar to that of $NO_x$.

Although the traffic modeling outcomes are theoretical estimations, the SCS and SBC top results for $CO_2$, CO, HC, $SO_x$ and PM match the places where the CETESB fixed stations show a substantial increase in the $O_3$ and $PM_{10}$ daily limits, exceeding the standards between 2015 and 2018, bearing in mind that HC, CO, and $NO_x$ are major precursors to $O_3$.

### 3.5.3. Chemical composition of mixed deposition

Rainwater analysis at the sampling stations in the PAR district, a preserved area in the urban area of SA, and the CAP local near Capuava Petrochemical Complex, allowed the quantification of chloride ($Cl^-$), nitrate ($NO_3^-$), sulfate ($SO_4^{2-}$), sodium ($Na^+$), ammonium ($NH_4^+$), potassium ($K^+$), magnesium ($Mg^{2+}$) and calcium ($Ca^{2+}$). Fluoride ($F^-$) was quantified in four samples, all of them at the CAP station (concentrations between 0.2 and 0.3 meq L$^{-1}$). The same was observed for phosphate ($PO_4^{3-}$), occurring in three samples from the CAP station with concentrations around 1.5 meq L$^{-1}$. The pH values similarly varied in both seasons, with minimum values of 4.2 and a maximum value of 7.5. The presence of cadmium (Cd) and lead (Pb) heavy metals in rainwater samples was also evaluated, and Fig. 11 presents the box-plot graphs of major ion and heavy metal concentrations in the two sampling stations.

For sulfate, the maximum values found for CAP are above those determined for PAR. Generally, $SO_4^{2-}$ may come from the oxidation of $SO_2$, primarily from the burning of fossil fuels containing residual sulfur contents. Higher sulfur levels in the CAP atmosphere can originate due to industrial activity in the area, typically oil refineries.

Among the chemical species analyzed, nitrate and calcium showed the highest variation between the sampling stations, with CAP values higher than those estimated in PAR. Nitrate ions in urban rainwater come from the oxidation of $NO_x$ emitted by burning fossil fuels used in the vehicle fleets. $Ca^{2+}$, $Mg^{2+}$, and $K^+$ cations in urban centers are generally associated with soil dust resuspension as well as civil construction activities.

These variations in concentrations were also observed in studies conducted in other metropolitan regions (Fornaro and Gutz, 2003; Leal et al., 2004; Vieira-Filho et al., 2015), highlighting the multiplicity of sources that contribute to pollution events in urban areas. To evaluate the possible contributions of the sources to the rainwater ionic species composition of the study area, the correlation matrix (Table 7) of the volume-weighted average for the determined ion concentrations was obtained.

The strong correlation (>0.8) observed between $H^+$ with sulfate and nitrate in rainwater collected in CAP indicates that the acidity found in these samples has contributions from strong acids such as sulfuric and nitric acids. The correlations between $H^+$ and anionic species for the samples collected in PAR were less significant, which may indicate predominant organic acid forms in the rainwater, such as formic and acetic monocarboxylic acids.

From the samples analyzed, 24% showed excess acidity with pH values lower than 5.6. The pH-weighted average value at the CAP station was 6.2 ± 0.9, which is very close to the average for PAR (6.0 ± 1.0). Although there are emissions of acidic species during the burning

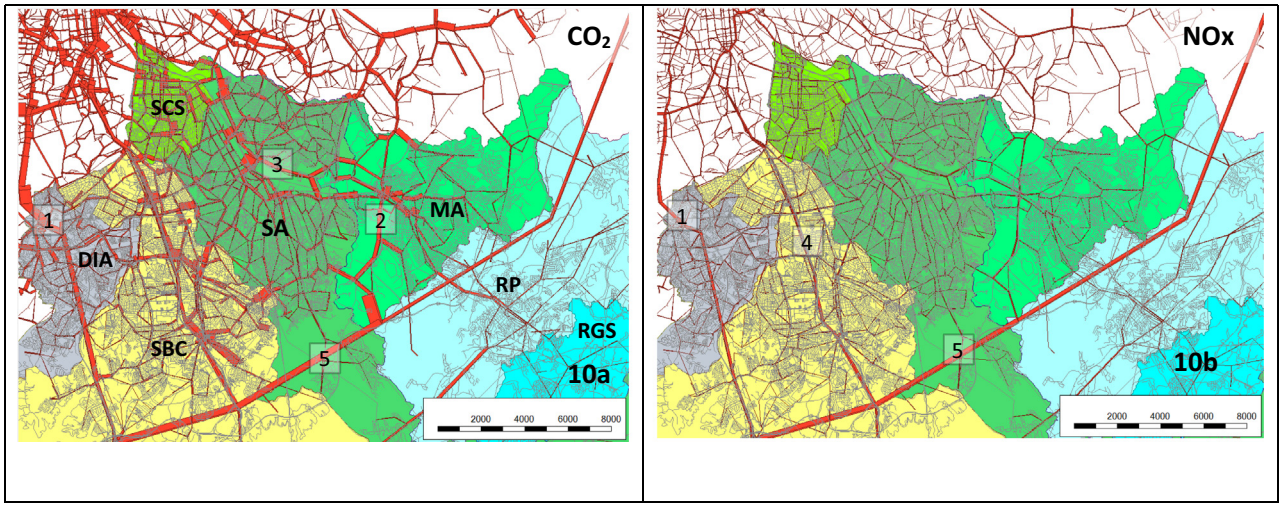


**Fig. 10.** Emissions by road segment of the urban area and traffic macrosimulation model (peak hours 7 AM – 8 AM) for $CO_2$ (a) and $NO_x$ (b). The numbers indicates the north-western stretch of Imigrantes highway (1), the Papa João XXIII Avenue (2), the Dos Estados Avenue (3), the Anchieta motorway (4) and the Rodoanel Mário Covas Orbital Motorway (5).

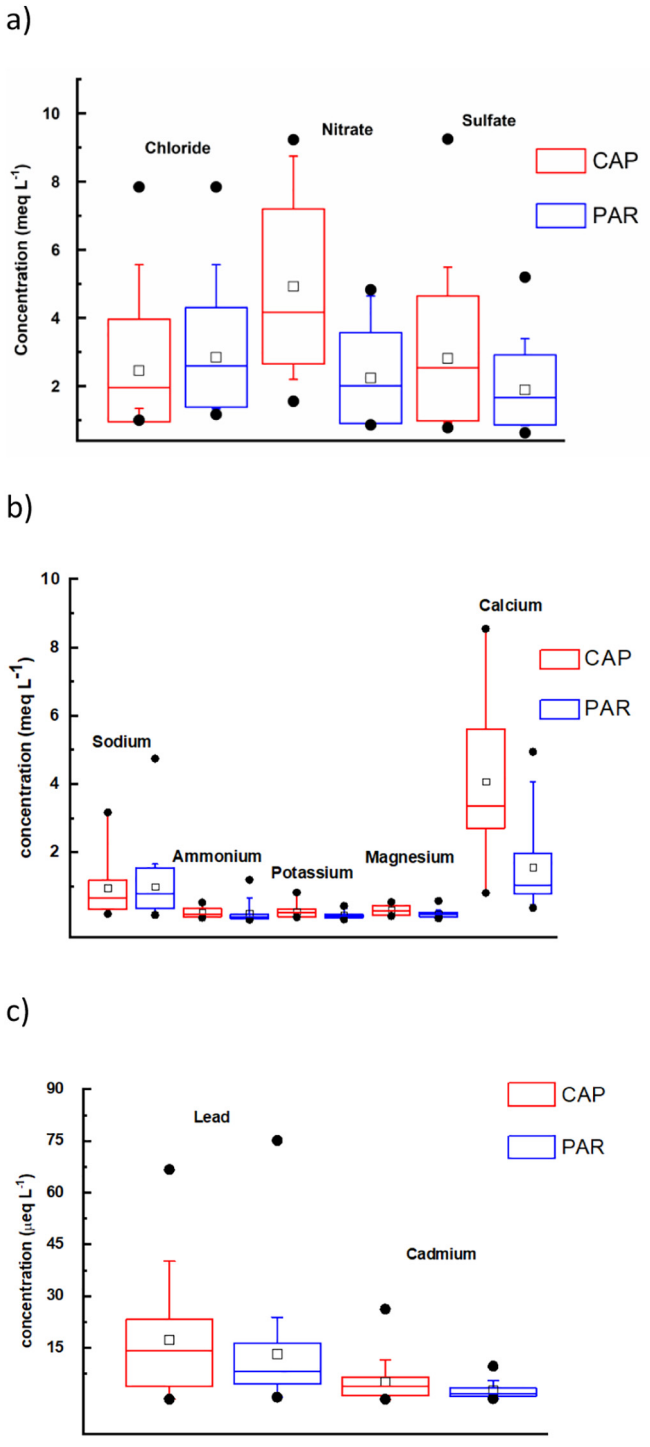


**Fig. 11.** Boxplot representation for concentrations of a) anions; b) cations (meq $L^{-1}$); and c) lead and cadmium (μeq $L^{-1}$); in mixed deposition samples from October 2016 to August 2017. The horizontal lines of the box express the values of 25, 50 and 75%. The error bar includes values between 5 and 95%; ● the minimum and maximum data set values and the arithmetic mean corresponds to the square within the box.

of fossil fuels, dust resuspension may lead to a partial neutralization of the sample acidity (Coelho et al., 2011).

Regarding the presence of heavy metals (Cd and Pb) in rainwater samples, the concentrations distribution is shown in Fig. 11c. Cadmium levels at the two sampling stations are statistically equivalent and do not show great variability, unlike lead. Comparing the concentration levels of these metals with those obtained for remote regions, which are considered uncontaminated, the Cd and Pb concentrations are,

**Table 7**
Correlation matrix between ionic species concentrations (in meq $L^{-1}$) determined in rainwater samples.

| | Capuava (CAP) | | | Paranapiacaba (PAR) | | |
|---|---|---|---|---|---|---|
| | $Cl^-$ | $NO_3^-$ | $SO_4^{2-}$ | $Cl^-$ | $NO_3^-$ | $SO_4^{2-}$ |
| $H^+$ | 0.26 | 0.85 | 0.82 | 0.21 | 0.58 | 0.47 |
| $Na^+$ | 0.89 | 0.19 | 0.12 | 0.81 | 0.27 | 0.34 |
| $NH_4^+$ | 0.23 | 0.26 | 0.60 | 0.49 | 0.49 | 0.62 |
| $K^+$ | 0.46 | 0.48 | 0.17 | 0.57 | 0.47 | 0.38 |
| $Mg^{2+}$ | 0.30 | 0.49 | 0.65 | 0.79 | 0.18 | 0.54 |
| $Ca^{2+}$ | 0.28 | 0.19 | 0.16 | 0.52 | 0.27 | 0.76 |

respectively, ten and five times higher in metropolitan regions (Chubaka et al., 2018).

To investigate the pollutants origins and dispersion that contributed to the rainwater chemical composition, the periods in which the concentrations of heavy metals (Cd and Pb) were above the mean concentration over the entire sample period were selected. Thus, it was found that the periods of the highest concentrations were from October 7th to 17th 2016 in Capuava, and from February 13th to 20th 2017 in Paranapiacaba.

Wind roses were built from hourly wind intensity and direction data for the periods identified (Fig. 12). The wind roses confirmed that emissions generated in the municipality of Cubatão reached the Paranapiacaba region. Cubatão borders SA, where there is a large industrial park with some predominant industrial processes: petrochemicals, fertilizers, non-metallic minerals, paper, and cement. In the past few decades, this municipality was considered the most polluted city in the world (Vieira-Filho et al., 2015). Given the geographical location of Paranapiacaba in relation to Cubatão, the former would be under the influence of Cubatão pollutant transport, according to the preferential SW wind direction (Fig. 12a). This was verified by the construction of the wind rose over four periods of the day (12:00–5:00 AM, 6:00–11:00 AM, 12:00–5:00 PM, and 6:00–11:00 PM). All of these time periods displayed SW winds, which indicates transportation of pollutants from Cubatão to Paranapiacaba, mostly in the afternoon (12:00–5:00 PM), when the winds were more intense compared to in other periods (Fig. 12b).

Fig. 12c shows the CETESB air quality stations at Capuava, in the municipality of SA, and the rainwater sampling station (CAP). The wind rose represents the sample period from October 7th to 17th 2016, when above average Cd and Pb concentration values occurred. There was a predominance of south-southeast winds (S-SSE) in the afternoon and evening and NW and NE winds in the morning. Considering that the wind conditions at the rainwater sample station (CAP) are like those at Capuava-CETESB, since the distance between them is 1.37 km, there is evidence of pollutants transport from Capuava Petrochemical Complex, which is located in the east-south quadrant of the sample station.

In addition, to the north of the rainwater sample station there is a large and heavily trafficked road, which connects SA with São Paulo. Thus, NE and NW winds should also contribute to pollutants from car fuel burn, suggesting that these may also be sources of pollutants recorded in the mixed deposition of CAP.

### 3.6. Principal component analysis

The PCA considered all previously analyzed atmospheric variables, for the 2015–2018 period on a monthly scale, in addition to the intensity of the HI, comfort index (THI), concentration of pollutants ($O_3$ and $PM_{10}$), and the number of days with pollutants exceeding the established limits ($N\_PM_{10}$ and $N\_O_3$).

In order to verify whether the PCA method is adequate for the purposes of this study, two statistical tests were performed: the Kaiser-Meyer-Oklin (KMO) test and the Barlett sphericity test (Kaiser, 1970). The KMO evaluates the adequacy of the sample with respect the degree

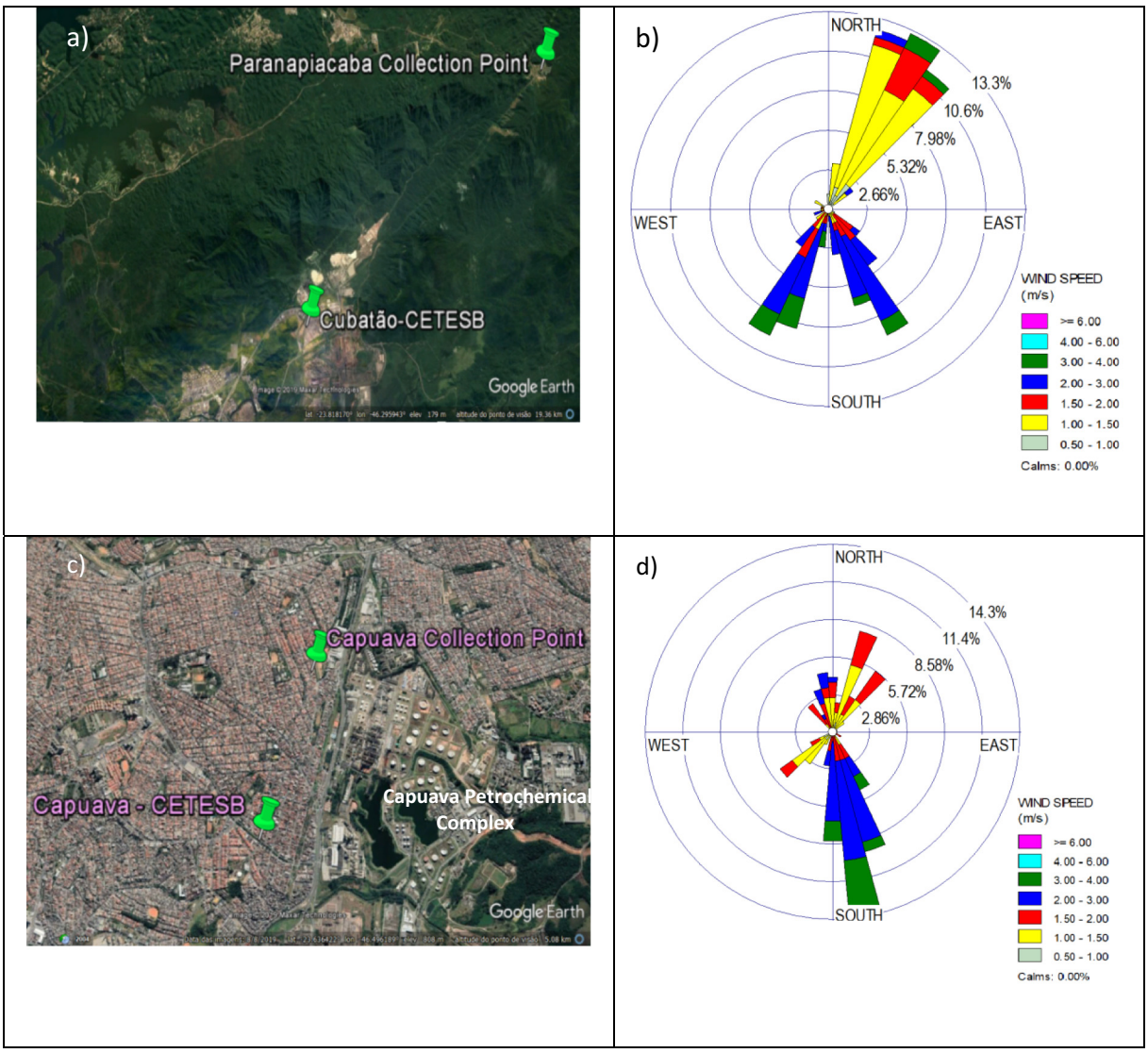


**Fig. 12.** Location of the sample stations of Paranapiacaba (a) and Capuava (c). Wind roses from hourly data of Cubatão -Vila Parisi – CETESB for February 13th to 20th 2017 periods (b) and Capuava - CETESB station for October 7th to 17th 2016 (d).

of partial correlation between the values, which should be small; the closer to 1 its value, the more appropriate the use of the technique. The result was a value of 0.76, which demonstrates that there is a good correlation between the variables. On the other hand, Bartlett's sphericity test rejected the null hypothesis that the data correlation matrix was an identity matrix ($p < 0.001$). Therefore, these results show

| Variables | PC1 | PC2 | PC3 |
|---|---|---|---|
| | Eigenvectors | | |
| THI | **0.92** | -0.21 | 0.12 |
| T | **0.90** | -0.17 | 0.04 |
| RH | -0.01 | **0.94** | -0.01 |
| HI | **0.79** | 0.18 | -0.21 |
| Wind | 0.29 | -0.08 | **-0.87** |
| PPP | **0.63** | 0.35 | -0.24 |
| $PM_{10}$ | **-0.57** | **-0.74** | -0.14 |
| $O_3$ | **0.78** | -0.39 | **0.19** |
| $N\_PM_{10}$ | -0.37 | **-0.75** | -0.23 |
| $N\_O_3$ | **0.66** | **-0.58** | **0.18** |
| **Eigenvalues** | 4.31 | 2.74 | 1.02 |

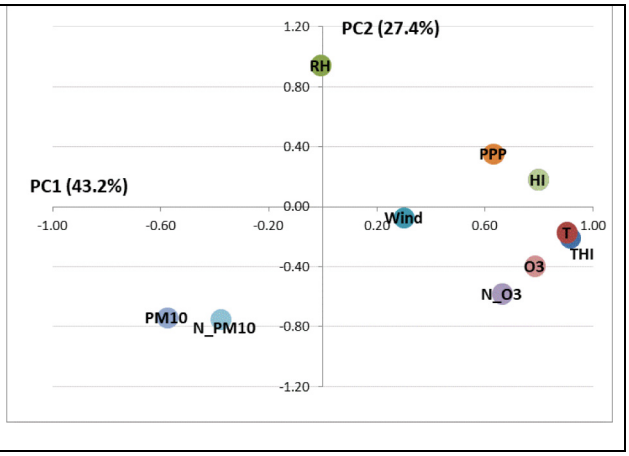


**Fig. 13.** Principal Components and the eigenvectors of the atmospheric and air quality variables analyzed for the urban area of ABC Paulista.

good fit of the data matrix to the factor analysis, indicating that analysis of principal components could indeed be performed.

The first three components (PC) explain 80.7% of the variance (eigenvalues) of the analyzed processes at, with 43.2%, 27.4% and 10.2% for the first, second, and third components, respectively. For the analysis of the first two components, eigenvectors greater than or equal to 0.5, either positive or negative, were selected (Fig. 13). PC1 presented the highest eigenvectors for variables related to air temperature (T), THI, and HI intensity, clearly representing the HI phenomenon associated with thermal comfort. In addition, PC1 supported the relationship among the $O_3$ concentrations, the number of days exceeding the limit, and the thermal characteristics associated with HI.

According to Freitas et al. (2007), there is a relationship between urban HI and its effects on pollutant dispersion in the MRSP, suggesting that during intense HI events the pollutant concentrations are higher. In the specific case of $O_3$, the high coefficient found in PC1 is also explained by high ozone levels (Fig. 8a) that occur close to the maximum daily solar radiation incidence, which also agrees with the period of the maximum intensity of HI between 2:00 PM and 4:00 PM. Unlike the $PM_{10}$ concentrations, where the maximum values occur at dawn (Fig. 8b), this may explain the negative coefficient for this pollutant found in PC1. The monthly rainfall (PPP) also presented a coefficient >0.5 suggesting that its intensity is also related to HI over the urban area of ABCP.

PC2 identified a strong and opposite relationship between the relative humidity (RH) and the concentrations of $PM_{10}$, N_$PM_{10}$, and N_$O_3$. This behavior can be explained when the sign of the coefficients is inverted and they are associated with lower RH conditions, especially in the winter season (Fig. 2a), and by the high concentrations of these pollutants. Studies show that, in the winter season, the number of days in which the limits are exceeded are higher, due to the absence of pollutant removal, mainly by wet deposition, and the association with stable atmospheric conditions (Santos et al., 2018; Freitas et al., 2007).

Studies that have analyzed the relationship between of atmospheric variables and pollutants in cities such as São Paulo (Santos et al., 2018) through the PCA methodology highlight that the low correlation values found for $PM_{10}$ and the atmospheric variables may be due to the high complexity of the processes involved. Some of these processes are not well recognized yet and differ from those associated with $O_3$, which has a strong dependence on radiation intensity. PM can act by decreasing or increasing the temperature, depending on its size and composition related to absorption or scattering mechanisms (Silva, 2012).

The inverse relationship of RH with $O_3$, with a low coefficient for this pollutant, may be related to ozone formation and depletion reactions. According to Seinfeld (1986), the presence of VOCs in the atmosphere with high relative humidity may lead to inhibition of $O_3$ formation. In an atmosphere with VOCs the destruction of $O_3$ may occur due to the reaction with peroxyl radicals formed through successive reaction routes of water vapor molecules. Another explanation would be associated with the lower RH values that usually occur during the highest radiation of the day, which coincides with higher ozone concentrations events.

The PC3 explains 10.2% of the data variance, highlighted by the wind intensity with the highest negative coefficient (−0.87) and the inverse relationship with $O_3$, and N_$O_3$ that showed the highest positive values for this component. Weak winds and no rain do not contribute to the dispersion of pollutants, consequently favoring a higher concentration and several days with favorable conditions to exceed the allowable limits, such as $O_3$, specifically for PC3.

## 4. Final considerations

The study of urban climate is interdisciplinary, as it involves several scientific fields. The UCS theoretical conceptual model developed by Monteiro and Mendonça (2003) sought to integrate most of the interacting processes, in order to explain atmospheric changes in urban areas, which this paper addresses. Aspects related to urban structure (verticality and waterproofing), the nature of building materials, as well as green areas and water bodies are not included in the model, however they are also important factors that determine urban climates.

The present work considered observed variables (atmospheric and air quality) from the ABCP urban area in order to identify the main atmospheric processes impacting the urban climate, such as the intensity of the HI, thermal comfort, locations with extreme rainfall, breeze patterns, and pollutant concentration conditions ($PM_{10}$ and $O_3$). To compare these characteristics, the period of 2015–2018 was chosen, and it was possible to identify the average main processes for the UCS in each municipality of the region.

The northern and northwestern regions of the ABCP urban area, which comprise the municipalities of DIA, SCS, and northern of SBC and SA, had the highest HI intensities, with DIA and SCS having the highest values in the spring and summer, characterized by a medium intensity HI in the afternoon. Thermal comfort indices, especially the THI, showed extreme discomfort levels in these municipalities in the summer.

Wind direction and intensity patterns were varied for each municipality, and frequent periods of sea breezes (SCS, SA, and SBC) and land breeze (DIA) were identified. In DIA, winds were less intense in the summer, making ventilation difficult, contributing to high temperatures and HIs.

Areas with higher frequencies of extreme rain events were identified by cluster analysis, and two groups related to excessive rainfall stood out. One of the groups includes DIA and SA-CA (in the northeastern area of SA) rain gauges, which showed higher daily precipitation values (average, maximum, and 85th and 95th percentiles). This suggests the occurrence of concentrated and heavy rainfall in these locations. These sites presented the hottest atmospheric conditions, with the highest HI intensity in DIA. Warmer atmospheric conditions are more unstable, providing more intense convergent movements for the formation of rain clouds.

The analysis of pollutant emissions based on CETESB fixed points was limited, as only two compounds were studied ($O_3$ and $PM_{10}$). Results showed that, on average, MA presented the highest $O_3$ concentration in October, followed by DIA.

With respect to $PM_{10}$ from 2015 to 2018, the municipalities of SCS and MA presented the maximum average concentrations value (50.8 $\mu g\ m^{-3}$) in July. This value indicates moderate air quality, according to the CETESB. On the other hand, although SCS had the highest average value, MA presented the largest number of days exceeding the permissible legal limit (until 2014). After this year, SCS presented the highest values.

These pollutants ($O_3$ and $PM_{10}$) contribute to the anthropogenic heat flux increase in urban areas, from vehicular and industrial emissions, and they can be considered to be partially responsible for the HIs in urban areas. Other factors such as surface coverage should be investigated in future work, due to the increase in sensible heat and reduction in latent heat (evaporation effects) in vegetated areas.

The emissions simulation, using traffic models provides new insights about pollutants spatial patterns, derived from mobile sources. Results expressed in kg $km^{-1}$ for each city showed that SCS has the highest emissions rates, followed by SBC and MA. Because SCS is the smallest city of ABCP, its rate of vehicle usage surpasses that of the others, with an average of 1.5 inhabitants per vehicle in SCS. Thus, the results of the emissions model simulations show, specifically for $CO_2$, $NO_x$, HC, and CO gases, that the municipalities of SCS, SBC, and MA have the highest emissions per km and are also some of the municipalities that had the highest HI intensities.

Regarding the rainwater chemical composition, there was evidence of excessive acidity levels (sulfuric and nitric acid) at the Capuava site, which is consistent with the simulations found by the transportation and emissions models. This also supported that the boundary of MA and SA were the high emission areas of these compounds. The presence

of $SO_4^{2-}$ comes from the oxidation of $SO_2$, mainly from burning fossil fuels containing residual sulfur. Capuava had the highest proportion of heavy metals in rainwater samples, such as lead, and the study identified its emission sources as the oil refineries and the main traffic routes that link important cities within the study region.

Finally, the PCA statistically verified the relationship between the observed variables and the main processes that explain the urban climate through the first three components with an explained variance of 80.7%. These are the intensity of the HI, thermal comfort, concentration of pollutants ($O_3$ and $PM_{10}$) associated with the number of days exceeding the legal limits, and process of dispersion of these pollutants in conditions of low relative humidity and in the absence of precipitation.

Detailed studies should be developed for specific periods where extreme conditions of the analyzed variables have been recorded, as it directly impacts the air quality and population health. An example of this extreme condition was observed on January 2, 2019, when the HI intensity reached 7.6 °C in SCS.

This study can provide essential information to investigate the role of HI and air pollution on mortality in these specific areas of the ABCP region and can inform policy-makers about more vulnerable areas to address public interventions targeting HI and acute air pollution episodes.

## CRediT authorship contribution statement

**María Cleofé Valverde:** Project administration, Formal analysis, Methodology, Data curation. **Lúcia Helena Coelho:** Formal analysis, Writing - original draft, Methodology. **Andréa de Oliveira Cardoso:** Methodology, Formal analysis. **Humberto Paiva Junior:** Writing - original draft, Methodology, Software. **Ricardo Brambila:** Formal analysis, Data curation. **Cláudia Boian:** Resources, Formal analysis. **Paula Cristina Martinelli:** Resources. **Natasha Murgu Valdambrini:** Resources.

## Declaration of competing interest

The authors declare that they have no known competing financial interests or personal relationships that could have appeared to influence the work reported in this paper.

## Acknowledgements

The authors acknowledges financial support from Fundação de Amparo à Pesquisa do Estado de São Paulo (FAPESP); Grant number 2016/14563-5.

## References

Alvim, D.S., Gatti, L.V., Corrêa, S.M., Chiquetto, J.B., Santos, G.M., Souza, R.C., Pretto, A., Rozante, J., Figueroa, S.N., Pendharkar, J., Nobre, P., 2018. Determining VOCs reactivity for ozone forming potential in the megacity of São Paulo. Aerosol Air Qual. Res. 18, 2460–2474. https://doi.org/10.4209/aaqr.2017.10.0361.

Andrade, M.d.F., Kumar, P., de Freitas, E.D., Ynoue, R.Y., Martins, J., Martins, L.D., Nogueira, T., Perez-Martinez, P., de Miranda, R.M., Albuquerque, T., Gonçalves, F.L.T., Oyama, B., Zhang, Y., 2017. Air quality in the megacity of São Paulo: evolution over the last 30 years and future perspectives. Atmos. Environ. 159, 66–82. https://doi.org/10.1016/j.atmosenv.2017.03.051.

Arnfield, A.J., 2003. Two decades of urban climate research: a review of turbulence, exchanges of energy and water, and the urban heat island. Int. J. Climatol. 23, 1–26. https://doi.org/10.1002/joc.859.

Associação Nacional de Transportes Públicos (ANTP), 2014. Estudo Comparativo de Tecnologias Veiculares de Tração Aplicadas a Ônibus Urbanos. Série Cadernos Técnicos, 15, 22, 2014. http://www.emtu.sp.gov.br/ftp/Caderno%20Tecnico%20-%20Vol%2015.pdf.

Atkinson, B.W., 1981. Meso-scale Atmospheric Circulations. London Academic Press (495 p., Chap. 5 & 6).

Auer, A.H., 1978. Correlation of land use and cover with meteorological anomalies. J. Appl. Meteorol. 17, 636–643. https://doi.org/10.1175/1520-0450(1978)017<0636:COLUAC>2.0.CO;2.

Barbirato, G.M., Souza, L.C.L., Torres, S.C., 2007. Clima e Cidade: a Abordagem Climática como Subsídios. EDUFAL, Maceió/AL (164 p).

Barros, H.R., Lombardo, M.A., 2016. A ilha de calor urbana e o uso e cobertura do solo em São Paulo. Geousp – Espaço e Tempo (Online) 20 (1), 160–177. https://doi.org/10.11606/issn.2179-0892.geousp.2016.97783.

Boian, C., Brumatti, M.M., Fornaro, A., 2015. Avaliação preliminar das concentrações de COV no entorno do Polo Petroquímico de Capuava, Mauá – SP. Revista Hipótese, Itapetininga 1 (2), 15–28. https://drive.google.com/file/d/0B4VVtZy9vhzvOHJ3Q0l1cV8tNlk/view.

Brena, N.A., 2002. A chuva Ácida e os seus Efeitos sobre as Florestas. São Paulo. 74 p. http://www.nilsonantoniobrena.com.br/a_chuva_acida.pdf.

Cardoso, R.S., Amorim, M.C.C.T., 2018. Urban heat island analysis using the 'local climate zone' scheme in Presidente Prudente, Brazil. Investig. Geográficas. 69, 107–118. https://doi.org/10.14198/INGEO2018.69.07.

Castanho, A.D., 1999. The Quantitative Determination of Sources of Particulate Matter in the Atmosphere of the City of São Paulo. PhD Dissertation. Institute of Physics, University of São Paulo, São Paulo, Brazil, p. 131. https://www.teses.usp.br/teses/disponiveis/43/43131/tde-19122003-145359/publico/TesemestradoAndreaPoluicaoSaoPaulo.pdf (accessed 04.06.2020).

CETESB, 2016. Companhia de Tecnologia de Saneamento Ambiental, 2015. Relatório de qualidade do ar no Estado de São Paulo 2015, Report of air quality in the São Paulo State 2015. accessed 02.03.2016. http://ar.cetesb.sp.gov.br/publicacoes-relatorios/.

CETESB, 2019. Companhia de Tecnologia de Saneamento Ambiental. Relatório de qualidade do ar no Estado de São Paulo 2018, Report of air quality in the São Paulo State 2018, 214 p. (accessed 21.09.2018). http://ar.cetesb.sp.gov.br/publicacoes-relatorios/.

Chubaka, C., Whiley, H., Edwards, J., Ross, K., 2018. Lead, zinc, copper, and cadmium content of water from south Australian rainwater tanks. Int. J. Environ. Res. Public Health 15 (7), 1551. https://www.mdpi.com/1660-4601/15/7/1551.

Coelho, C.H., Allen, A.G., Fornaro, A., Orlando, E.A., Grigoletto, T.B., Campos, M.L.M., 2011. Wet deposition of major ions in a rural area impacted by biomass burning emissions. Atmos. Environ. 45 (32), 5260–5265. https://doi.org/10.1016/j.atmosenv.2011.06.063.

Coelho, M.S., Boian, C., Fornaro, A., Nogueira, T., de Sales, C., 2017. Hydrocarbons (C6-C11) concentration around the petrochemical complex in the great ABC region, São Paulo, Brazil. Air Quality Conference Brazil - CMAS South America, 2017, Vitória. Fundação Espírito Santense de Tecnologia, Espírito Santo.

Dayan, U., Lamb, D., 2003. Meteorological indicators of summer precipitation chemistry in central Pennsylvania. Atm. Environ. 37 (8), 1045–1055. https://doi.org/10.1016/S1352-2310(02)00992-5.

Deryugina, T., Heutel, G., Miller, N.H., Molitor, D., Reif, J., 2019. The mortality and medical costs of air pollution: evidence from changes in wind direction. Am. Econ. Rev. 109 (12), 4178–4219.

Duarte, L.H.K. Paiva Junior, H. 2013. Inventário de emissões por fontes móveis em cidades de pequeno e médio porte. In: Tobias, M.S.G. e Lima, A.C.M. Urbanização & Meio Ambiente. Belém. Unama – Universidade da Amazônia. vol. 2, 451–436.

Fernandes, R.A., Valverde, M.C., 2017. Análise da resiliência aos extremos climáticos de chuva: estudo preliminar na região de Mauá no ABC Paulista, São Paulo. Revista Brasileira de Ciências Ambientais - RBCIAM 44, 1–17. https://doi.org/10.5327/Z2176-947820170183.

Fornaro, A., Gutz, I.G.R., 2003. Wet deposition and related atmospheric chemistry in the Sao Paulo metropolis, Brazil: part 2—contribution of formic and acetic acids. Atmos. Environ. 37 (1), 117–128. https://doi.org/10.1016/S1352-2310(02)00885-3.

Freitas, E.D., Silva Dias, P.L., Rozoff, C.M., Cotton, W.R., 2007. Interactions of an urban heat island and sea-breeze circulations during winter over the metropolitan area of Sao Paulo, Brazil. Boundary-Layer Meteorol 122 (1), 43–65. https://doi.org/10.1007/s10546-006-9091-3.

Garcia, F.F., 1996. Manual de climatologia aplicada: clima, medio ambiente y planificación. Editorial Síntesis, S.A, Madrid (285p).

Grimmond, S., 2007. Urbanization and global environmental change: local effects of urban warming. Geogr. J. 173, 83–88. https://doi.org/10.1111/j.1475-4959.2007.232_3.x.

IBGE, 2019. Instituto Brasileiro de Geografia e Estatística (Brazilian Institute of Geography and Statistics). Estimativa da população residente no Brasil. Diretoria de Pesquisas - DPE. 2010 . http://www.ibge.gov.br, Accessed date: 9 April 2019.

IPCC, 2007. In: Solomon, S., Qin, D., Manning, M., Chen, Z., Marquis, M., Averyt, K.B., Tignor, M., Miller, H.L. (Eds.), Climate Change 2007: The Physical Science Basis. Contribution of Working Group I to the Fourth Assessment Report of the Intergovernmental Panel on Climate Change. Cambridge University Press, Cambridge, United Kingdom and New York, NY, USA 996 pp. https://www.ipcc.ch/site/assets/uploads/2018/05/ar4_wg1_full_report-1.pdf.

IPEA, ANTP, 1999. Redução das deseconomias urbanas com a melhoria do transporte público. Revistas dos Transportes - ANTP. Ano 21, 35–92. http://files-server.antp.org.br/_5dotSystem/download/dcmDocument/2013/01/10/057A84C9-76D1-4BEC-9837-7E0B0AEAF5CE.pdf.

Kaiser, H., 1970. A second generation Little Jiffy. Psychometrika 35, 401–415.

Kermanshah, A., Derrible, S., Berkelhammer, M., 2017. Using climate models to estimate urban vulnerability to flash floods. J. Appl. Meteorol. Climatol. 56 (9), 2637–2650. https://doi.org/10.1175/JAMC-D-17-0083.1.

Leal, T.F.M., Fontenele, A.P.G., Pedrotti, J.J., Fornaro, A., 2004. Composição iônica majoritária de águas de chuva na região central de São Paulo. Quím. Nova. 27 (6), 851–855. https://doi.org/10.1590/S0100-40422004000600003.

Marengo, J.A., Valverde, M.C., Obregón, G., 2013. Observed and projected changes in rainfall extremes in the Metropolitan Area of São Paulo. Clim. Res. 57, 61–72. https://doi.org/10.3354/cr01160.

Martins, L.D., Andrade, M.F., 2008. Ozone formation potentials of volatile organic compounds and ozone sensitivity to their emission in the megacity of Sao Paulo, Brazil. Water Air Soil Pollut. 195 (1), 201–213. https://doi.org/10.1007/s11270-008-9740-x1.

Molina, E.A., Cardoso, A.O., Nogueira, F.R., 2015. Relação Precipitação-Deslizamento no Município de São Bernardo do Campo – SP. Ciência e Natura 37, 46–54. https://doi.org/10.5902/2179460X16214.

Monteiro, C.A., Mendonça, F., 2003. Clima Urbano. Editora Contexto (192p).

Moro Junior, E., 2007. A redenção inexistente nos planos urbanísticos municipais: o caso do Projeto Eixo Tamanduatehy. Annablume, São Paulo (114p).

Nobre, C.A., Young, A.F., Marengo, J.A., Saldiva, P.H.N., Nobre, A.D., Ogura, A.T., Thomaz, O., Valverde, M.C., Obregón, G., Moreira da Silva, G.C., Silveira, A.C., Rodrigues, G.O., 2011. Vulnerabilidades das Megacidades Brasileiras às Mudanças Climáticas: Região Metropolitana de São Paulo. In: Ronaldo Seroa da Motta; Jorge Hargrave; Gustavo Luedemann; Maria Bernadete Sarmiento Gutierrez. (Org.). Mudança do clima no Brasil: aspectos econômicos, sociais e regulatórios. 1 ed. Brasília: IPEA, p. 233–257.

Nóbrega, R.S., Lemos, T., 2011. O microclima e o (des)conforto térmico em ambientes abertos na cidade do recife. Revista de Geografia (UFPE) 28 (1), 93–109. https://www3.ufpe.br/tropoclima/images/pdf/nobrega.pdf.

Oke, T.R., 1987. Street design and urban canopy layer climate. Energy and Buildings 11, 103–113. https://doi.org/10.1016/0378-7788(88)90026-6.

Oke, T.R., et al., 1999. The energy balance of central Mexico City during the dry season. Atmos. Environ. 33 (24/25), 3919–3930. https://doi.org/10.1016/S1352-2310(99)00134-X.

Oliveira, A.P., Bornstein, R., Soares, J., 2003. Annual and diurnal wind patterns in the city of Sao Paulo. Water Air Soil Pollut. 3, 3–15. https://doi.org/10.1023/A:1026090103764.

Ono, H.S.P., Kawamura, T., 1991. Sensible climates in monsoon Asia. Int. J. Biometeorol. 35 (1), 39–47. https://doi.org/10.1007/BF01040962.

Peng, S., Piao, S., Ciais, P., Friedlingstein, P., Ottle, C., Breon, F.M., Nan, H., Zhou, L., Myneni, R.B., 2012. Surface urban heat island across 419 global big cities. Environ. Sci. Technol. 46, 696–703. https://doi.org/10.1021/es2030438.

Santamouris, M., Haddad, S., Fiorito, F., Osmond, P., Ding, L., Prasad, D., Zhai, X., Wang, R., 2017. Urban heat island and overheating characteristics in Sydney, Australia. An analysis of multiyear measurements. Sustainability 9 (5), 712. https://doi.org/10.3390/su9050712.

Santos, M.A., Illanes, C.F., Fornaro, A., Pedrotti, J.J., 2007. Acid rain in downtown São Paulo City. Brazil. Water Air Soil Pollut: Focus. 7, 85–92. https://doi.org/10.1007/978-1-4020-5885-1_10.

Santos, T.C., Reboita, M.S., Carvalho, V.S.B., 2018. Investigação da Relação entre Variáveis Atmosféricas e a Concentração de $MP_{10}$ e $O_3$ no Estado de São Paulo. Rev. Bras. Meteorol. 33, 631–645. https://doi.org/10.1590/0102-778633400.

Seinfeld, J.H., 1986. Atmospheric Chemistry and Physics of Air Pollution. John Willey & Sons, New York (1152p).

Silva, B.L., 2012. Estudo do efeito das partículas de aerossol emitidas por queimadas sobre a radiação solar incidente em superfície a partir de medições efetuadas na Reserva Biológica do Jaru. 2012. Dissertação (Mestrado em Meteorologia) - Instituto de Astronomia, Geofísica e Ciências Atmosféricas, Universidade de São Paulo. São Paulo - SP (119 p).

Silva Dias, M.A.F., Dias, J., Carvalho, L.M.V., Freitas, E.D., Silva Dias, P.L., 2012. Changes in extreme daily rainfall for São Paulo, Brazil. Clim. Chang. 116, 705–722. https://doi.org/10.1007/s10584-012-0504-7.

Simeão, A.B., Scopel, S.B., Valverde, M.C., 2019. Estudo da ilha de calor urbana atmosférica em São Bernardo do Campo - SP e propostas de mitigação. Revista Hipótese 5 (1), 671–698. https://nutecca.webnode.com/_files/200000137-c7980c895e/ESTUDO%20DA%20ILHA%20DE%20CALOR%20URBANA%20ATMOSF%C3%89RICA%20EM%20S%C3%83O%20BERNARDO%20DO%20CAMPO-SP%20E%20PROPOSTAS%20DE%20MITIGA%C3%87%C3%83O.pdf.

Tabony, R.C., 1983. The estimation of missing climatological data. Int. J. Climatol. 3 (3), 297–314. https://doi.org/10.1002/joc.3370030308.

Tran, H., Uchihama, D., Ochi, S., Yasuoka, Y., 2006. Assessment with satellite data of the urban heat island effects in Asian mega cities. Int. J. Appl. Earth Obs. Geoinf. 8 (1), 34–48. https://doi.org/10.1016/j.jag.2005.05.003.

UNEP, 2011. Near-term Climate Protection and Clean Air Benefits: Actions for Controlling Short-lived Climate Forcers. United Nations Environment Programme (UNEP), Nairobi, Kenya, p. 78. http://wedocs.unep.org/handle/20.500.11822/8048, Accessed date: 5 March 2020.

Valero, F., Gonzalez, F.J.D., García-Miguel, J.A., 1996. A method for the reconstruction and temporal extension of climatological time series. Int. J. Climatol. 16, 213–227. https://doi.org/10.1002/(SICI)1097-0088(199602)16:2<213::AID-JOC996>3.0.CO;2-7.

Valverde, M.C., 2017. The interdependence of climate and socioeconomic vulnerability in the ABC Paulista region. Ambiente & Sociedade 20 (3), 39–60. https://doi.org/10.1590/1809-4422asoc66r2v2032017.

Valverde, M.C., Cardoso, A., Brambila, R., 2018. O padrão de chuvas na região do ABC Paulista: os extremos e seus impactos. Rev. Bras. de Climatologia. 22, 165–187. https://doi.org/10.5380/abclima.v22i0.45929.

Valverde, M.C., Paiva Junior, H., 2018. Temperatura do ar e emissões urbanas em região industrial de São Paulo, Brasil. Acta Brasiliensis 2 (2), 45–52. http://revistas.ufcg.edu.br/ActaBra/index.php/actabra/article/view/90/44.

Vieira-Filho, M.S., Lehmann, C., Fornaro, A., 2015. Influence of local sources and topography on air quality and rainwater composition in Cubatão and São Paulo, Brazil. Atmos. Environ. 101, 200–208. https://doi.org/10.1016/j.atmosenv.2014.11.025.

Wilks, D.S., 2006. Statistical Methods in the Atmospheric Sciences. 2nd ed. Academic Press, London 634p. http://danida.vnu.edu.vn/cpis/files/Books/Statistical%20methods%20in%20the%20atmospheric%20sciences%20D.%20Wilks%20(2ed.,%20IGS%2091,%20Elsevier,%202006)(ISBN%200127519661)(649s).pdf.

WMO, 2019. WMO Statement on the State of the Global Climate in 2018. WMO-No. 1233. accessed on 04.10.2019. https://library.wmo.int/doc_num.php?explnum_id=5789.

Xavier, T.M., Xavier, A.F.S., Silva Dias, M.A.F., 1994. Evolução da precipitação diária num ambiente urbano: o caso da Cida de São Paulo. Rev. Bras. Meteorol. 9 (1), 44–53.